Effects of foliage clumping on the estimation of global terrestrial gross primary productivity

Jing M. Chen,[1,2] Gang Mo,[2] Jan Pisek,[2,3] Jane Liu,[2] Feng Deng,[1] Misa Ishizawa,[4] and Douglas Chan[4]

Received 16 November 2010; revised 22 November 2011; accepted 3 January 2012; published 1 March 2012.

[1] Sunlit and shaded leaf separation proposed by Norman (1982) is an effective way to upscale from leaf to canopy in modeling vegetation photosynthesis. The Boreal Ecosystem Productivity Simulator (BEPS) makes use of this methodology, and has been shown to be reliable in modeling the gross primary productivity (GPP) derived from CO_2 flux and tree ring measurements. In this study, we use BEPS to investigate the effect of canopy architecture on the global distribution of GPP. For this purpose, we use not only leaf area index (LAI) but also the first ever global map of the foliage clumping index derived from the multiangle satellite sensor POLDER at 6 km resolution. The clumping index, which characterizes the degree of the deviation of 3-dimensional leaf spatial distributions from the random case, is used to separate sunlit and shaded LAI values for a given LAI. Our model results show that global GPP in 2003 was 132 $\pm$ 22 Pg C. Relative to this baseline case, our results also show: (1) global GPP is overestimated by 12% when accurate LAI is available but clumping is ignored, and (2) global GPP is underestimated by 9% when the effective LAI is available and clumping is ignored. The clumping effects in both cases are statistically significant ($p < 0.001$). The effective LAI is often derived from remote sensing by inverting the measured canopy gap fraction to LAI without considering the clumping. Global GPP would therefore be generally underestimated when remotely sensed LAI (actually effective LAI by our definition) is used. This is due to the underestimation of the shaded LAI and therefore the contribution of shaded leaves to GPP. We found that shaded leaves contribute 50%, 38%, 37%, 39%, 26%, 29% and 21% to the total GPP for broadleaf evergreen forest, broadleaf deciduous forest, evergreen conifer forest, deciduous conifer forest, shrub, C4 vegetation, and other vegetation, respectively. The global average of this ratio is 35%.

Citation: Chen, J. M., G. Mo, J. Pisek, J. Liu, F. Deng, M. Ishizawa, and D. Chan (2012), Effects of foliage clumping on the estimation of global terrestrial gross primary productivity, *Global Biogeochem. Cycles*, *26*, GB1019, doi:10.1029/2010GB003996.

1. Introduction

[2] The terrestrial carbon cycle is the most variable component of the global carbon cycle [*Canadell et al.*, 2007; *Le Quéré et al.*, 2009], contributing most to the interannual variability of the atmospheric CO_2 concentration [*Zhao and Running*, 2010]. However, our ability to estimate the quantity of the terrestrial carbon sink and its interannual variability is still limited, and the estimates are still uncertain [*Gurney et al.*, 2002; *Baker et al.*, 2006; *Rayner et al.*, 2008], especially with process-based ecosystem models [*Schulze and Schimel*, 2001; *Schwalm et al.*, 2010]. This makes it unreliable to assess the possible changes in the terrestrial carbon cycle under future climate scenarios [*Friedlingstein et al.*, 2006].

[3] The variability of the terrestrial carbon cycle is caused mainly by the variable rates of plant growth and fire and insect disturbance under variable weather conditions. The gross primary productivity (GPP), quantifying the rate of carbon uptake from the atmosphere through photosynthesis, is arguably the most variable component of the terrestrial carbon cycle, and our ability to model this component accurately is critical in global carbon cycle and climate research. *Cramer et al.* [1999] carried out the first comprehensive research on global net primary productivity (NPP) and found that NPP estimated by terrestrial ecosystem models of varying complexity ranged between 44.4 and 66.3 Pg C y^{-1}. NPP is GPP minus autotrophic respiration and is about 47% of GPP [*Ruimy et al.*, 1996]. Various estimates of the global GPP have been reported, including

[1]International Institute of Earth System Science, Nanjing University, Nanjing, China.
[2]Department of Geography, University of Toronto, Toronto, Ontario, Canada.
[3]Tartu Observatory 61602, Toravere, Estonia.
[4]Meteorological Service of Canada, Environment Canada, Toronto, Ontario, Canada.

0886-6236/12/2010GB003996

(1) 133 Pg C y^{-1} by *Ruimy et al.* [1996]; (2) 129 Pg C y^{-1} by *Demarty et al.* [2007]; (3) 107–167 Pg C y^{-1} by *Knorr and Heimann* [2001] and *Cramer et al.* [2001]; and (4) 123 ± 8 Pg C y^{-1} by *Beer et al.* [2010]. These estimates differ considerably because of different data sets used and different ways of estimating photosynthesis. *Alton et al.* [2007] conducted an interesting study to compare global GPP values estimated using different photosynthesis models with the same data inputs. They showed that the global GPP is estimated to be 129–131 Pg C y^{-1} by a big-leaf model, which treats a canopy as a big-leaf, but it is 118 Pg C y^{-1} by a sunlit-shaded leaf model, which separates a canopy into sunlit and shaded leaf groups. This study suggests that the way that photosynthesis is estimated at the canopy level would be the main cause of global GPP estimation uncertainty, given accurate input data sets.

[4] Since the pioneering works of *Norman and Jarvis* [1974], *Norman* [1982], and *Norman and Welles* [1983], among others, canopy-level photosynthesis modeling has advanced considerably in the last decade or so. It is now clearly recognized that big-leaf models are conceptually flawed and practically inaccurate [*Chen et al.*, 1999] and sunlit-shaded leaf stratification is necessary to make accurate canopy-level GPP estimation [*De Pury and Farquhar*, 1997; *Wang and Leuning*, 1998]. For sunlit and shaded leaf stratification, we need accurate description of the canopy structure with at least two structural parameters. One is the leaf area index (LAI), defined as one half the total (all sided) leaf area per unit ground surface area [*Chen and Black*, 1992]. The other is the foliage clumping index characterizing the way that leaves in a canopy are spatially organized. Leaves in canopies are generally grouped into various sub-canopy structures, such as tree crowns, branches, and shoots in forests, foliage clumps in shrubs, and rows in crops. These structures make the leaf spatial distribution non-random, and the foliage clumping index is used to quantify the degree of the deviation of this distribution from the random case. In addition to LAI, the foliage clumping index is also an important parameter for accurate separation of sunlit and shaded leaf groups and for accurate canopy-level GPP modeling [*Chen et al.*, 2003]. For the same LAI, there will be fewer sunlit leaves and more shaded leaves if the leaf distribution is clumped. As photosynthetic rates of shaded leaves are generally 2–3 times lower than those of sunlit leaves, we would expect that foliage clumping has a considerable effect on the canopy-level GPP. In fact, vascular plants may have evolved to have canopy architectures that can optimize the total canopy photosynthesis under given light conditions [*Schieving*, 1998]. This optimization would be achieved through maximizing the contribution from shaded leaves receiving diffuse irradiance in clumped canopies [*Sterck and Schieving*, 2007], as the contribution of sunlit leaves is mostly limited by the direct irradiance.

[5] Through multiangle remote sensing, the first ever global clumping index map has been produced at 6 km resolution [*Chen et al.*, 2005], although some regional maps were produced using a different methodology [*Roujean and Lacaze*, 2002]. This provides an opportunity to conduct sunlit and shaded leaf photosynthesis modeling at the global scale in a meaningful way. The purpose of this study is to assess the importance of canopy architecture characterization in global GPP estimation. It will be demonstrated through this assessment that accurate mapping of vegetation structure in terms of both the foliage amount (LAI) and the foliage organization pattern (clumping) should be pursued as we work to improve global GPP estimation. Although rigorous validation of the coarse resolution global clumping index map must be deferred until high-resolution multiangle satellite sensors become available, it is our intention that through this explorative study we raise the awareness of the foliage clumping issue in global carbon cycle research in order to stimulate remote sensing technological development useful for clumping mapping.

2. Modeling Methodology

[6] The Boreal Ecosystem Productivity Simulator (BEPS) is used for global GPP modeling in this study. Although BEPS was initially developed for boreal ecosystems, it has been expanded and used for temperate and tropical ecosystems in Asia [*Matsushita and Tamura*, 2002; *Matsushita et al.*, 2004], China [*Feng et al.*, 2007], and Germany [*Wang et al.*, 2003]. BEPS was initially a daily model [*Liu et al.*, 1997; *Chen et al.*, 1999], developed based on Forest-BGC [*Hunt and Running*, 1992]. It was recently upgraded as an hourly model [*Ju et al.*, 2006] with a canopy energy balance module [*B. Chen et al.*, 2007]. BEPS follows the sunlit-shaded leaf stratification strategy [*Norman*, 1982] in modeling canopy-level photosynthesis. Various sunlit-shaded separated models, dubbed "two-leaf" models, are shown to be effective in canopy-level photosynthesis modeling [*Leuning et al.*, 1995; *De Pury and Farquhar*, 1997; *Wang and Leuning*, 1998]. Using simultaneous CO_2 flux measurements above and below two forest canopies, *Chen et al.* [1999] demonstrated that "big-leaf" photosynthesis models lack the ability to simulate day-to-day variations in canopy photosynthesis and a two-leaf model can avoid this problem (see more discussions in section 2.2).

2.1. Sunlit and Shaded LAI Separation

[7] The key to successful separation of sunlit and shaded leaf groups is accurate description of the canopy structure. Usually, LAI is the only structural parameter used for photosynthesis modeling and the angular and spatial distributions of leaves are assumed to be random. The assumption of random leaf angle distribution, i.e., the normals to leaves are distributed spherically, is often not met and can sometimes incur considerable error in radiation interception estimation [*Baldocchi et al.*, 2002]. For daily estimation, the random leaf angle distribution can often be a reasonable approximation, and even for well structured erectophile conifer forests, the error in radiation transmission estimation is within 20% [*Chen*, 1996a]. However, the assumption of the random leaf spatial distribution is generally seriously violated because of the sub-canopy structures [*Chen*, 1996b]. The effect of a non-random leaf spatial distribution on radiation transmission through an azimuthally symmetric canopy has been described using a leaf dispersion parameter Ω [*Nilson*, 1971]:

$$P(\theta) = e^{-G(\theta)\Omega L/\cos\theta} \quad (1)$$

where $P(\theta)$ is the probability of radiation transmission through the canopy at zenith angle θ, $G(\theta)$ is the projection

coefficient, defined as the area projected on a plane perpendicular to the direction of radiation per unit leaf area, and often taken as 0.5 for the random (spherical) leaf angle distribution, and L is the LAI. In plant canopies, the grouping of leaves in the sub-canopy structures causes more overlapping of leaves vertically or in any direction than the random case, and hence increases the probability of radiation transmission through the canopy. The more Ω departs from unity, the more non-random is the foliage spatial distribution. Clumping effectively reduces the influence of LAI on radiation interception, and therefore the Ω value is usually smaller than unity and is often referred to as "clumping index" [*Chen et al.*, 1991]. The product of Ω and L effectively determines the radiation transmission through the canopy, and therefore is called the effective LAI [*Chen et al.*, 1991].

[8] For a given canopy structure as described by L and Ω, the total LAI can be separated into sunlit LAI (L_{sun}) and shaded LAI (L_{sh}) for the purpose of canopy-level photosynthesis modeling using a two-leaf model. The method of *Norman* [1982] has been modified to consider the effect of foliage clumping on the sunlit and shaded LAI separation [*Chen et al.*, 1999]:

$$L_{sun} = 2\cos\theta\left(1 - e^{-0.5\Omega L/\cos\theta}\right) \tag{2a}$$

$$L_{sh} = L - L_{sun} \tag{2b}$$

It can be inferred from equation (2a) that as the foliage clumping increases (decreasing Ω value), L_{sun} decreases. This is because clumping, i.e., grouping of leaves, increases the probability of leaf overlapping from the random case, and as a result it decreases the probability of a leaf exposing to the direct light. This decrease in L_{sun} as a result of clumping leads to an increase in L_{sh} (equation (2b)). The typical values of Ω are 0.5–0.7 for conifer forests and 0.7–0.9 for broadleaf forests [*Chen*, 1996b; *Chen et al.*, 1997; *Ryu et al.*, 2010a]. For crops, limited Ω measurements fall in the range from 0.4 to 0.8 depending on the row structure [*Cohen et al.*, 1997; *Demarez et al.*, 2008]. For dense wetland grass and shrub, Ω is found to be close to unity [*Sonnentag et al.*, 2007]. As Ω is usually considerably smaller than unity (the random case), it is critically important to consider this factor in productivity models because foliage clumping alters the way plants interact with incident radiation. From the mathematical way that L and Ω are used in equation (2a), we can say that these two parameters are of equal importance in radiation modeling. However, LAI naturally has a larger variability than clumping, and would still be the most important parameter to be used in ecosystem models. The clumped architecture of forest canopies, in particular, makes the stratification between sunlit and shaded leaves essential. This is because the fraction of the shaded leaves is much larger in clumped canopies than in random canopies and shaded leaves play an important role in forest and shrub productivities [*Goulden et al.*, 1997; *Baldocchi and Harley*, 1995; *Chen et al.*, 2003].

2.2. Sunlit and Shaded GPP Modeling

[9] The methodology developed by *Chen et al.* [1999] for computationally efficient estimation of sunlit and shaded leaf irradiances is used in this study (Appendix A), and these irradiances are used for sunlit and shaded leaf photosynthesis estimation. To investigate the importance of foliage clumping in estimating photosynthetic carbon uptake, the photosynthesis rates of representative sunlit and shaded leaves need to be simulated separately. The canopy-level photosynthesis (A_{canopy}) can then be obtained as the sum of the total photosynthesis of sunlit and shaded leaf groups:

$$A_{canopy} = A_{sun}L_{sun} + A_{sh}L_{sh} \tag{3}$$

where the subscripts "sun" and "sh" denote the sunlit and shaded components of photosynthesis and LAI. This two-leaf formulation is based on the estimation of the photosynthesis rates of a representative sunlit leaf (A_{sun}) and a representative shaded leaf (A_{shade}). These photosynthesis rates are calculated using Farquhar's leaf biochemical model [*Farquhar et al.*, 1980]. This model can be combined with a physical model describing the CO_2 flow from the free air to the inside of the stomatal cavity [*Leuning*, 1990] for sunlit and shaded leaves separately [*Chen et al.*, 1999]. Some key parameters, the canopy-level mean maximum carboxilation rate (V_{cmax}) at 25°C and the maximum electron transport rate (J_{max}) of sunlit leaves, used in Farquhar's model, are provided in Table 1. The mean leaf nitrogen content, the standard deviation of V_{cmax} for each PFT are also provided in Table 1 for estimating the mean values of V_{cmax} and J_{max} for sunlit and shaded leaves separately according to vertical leaf nitrogen content gradient in the canopy (Appendix B).

[10] Using Leuning's method, the photosynthesis rate of a leaf can be estimated using Farquhar's model once the stomatal conductance of the leaf is known. *Ball* [1988] found that leaf stomatal conductance is linearly related to its photosynthesis rate (A, representing either A_{sun} or A_{sh}):

$$g = m\frac{Ah_s}{C_s}p + b \tag{4}$$

where g is stomatal conductance expressed in μmol m^{-2} s^{-1}, m is a plant species dependent coefficient (Table 1), h_s is the relative humidity at the leaf surface, p is the atmospheric pressure, C_s is the CO_2 concentration at the leaf surface, and b is a small value due to leaf dark respiration (Table 1). Equation (4) is often called Ball-Berry equation. As g is needed in A calculations and A is needed in g calculations (equation (4)), an iteration procedure is usually followed for simultaneous estimations of A and g [*Collatz et al.*, 1991]. In our model, g is obtained this way for sunlit and shaded leaves separately. We use an analytical solution of g [*Baldocchi*, 1994] in order to improve the computation efficiency for global simulations. The values of V_{cmax} in Table 1 for the various plant functional types (PFTs) except for C4 plants are adopted from *Kattge et al.* [2009] who conducted metadata analysis with 723 leaf-level V_{cmax} data points. The V_{cmax} and m values for C4 plants are obtained from *Hanan et al.* [2005]. The J_{max} values in Table 1 are estimated using the equation established by *Medlyn et al.* [1999a] through metadata analysis. The values of m for the various PFTs vary in a large range from 5 to 16, but we have chosen the most frequently used values.

[11] The intercept values b are generally very small and treated as a constant for all PFTs. It was shown that the big-

Table 1. Biochemical and Biophysical Parameters Used in BEPS for Various Plant Functional Types

Parameters[a]	Broadleaf Evergreen	Broadleaf Deciduous	Evergreen Conifers	Deciduous Conifers	Shrub	C4 Plants	Others	References
V_{cmax} μmol m^{-2} s^{-1} (at 25°C)	29.0 ± 7.7	57.7 ± 21.2	62.5 ± 24.7	39.1 ± 11.7	57.9 ± 19.6	100.7 ± 36.6	90.0 ± 89.5	*Wullschleger* [1993]; *Medlyn et al.* [1999a, 1999b]; *Niu et al.* [2005]; *Kattge et al.* [2009]
J_{max} μmol m^{-2} s^{-1}	55.1	123.7	135.2	79.2	124.1	193.1	200.0	*Medlyn et al.* [1999a]; *Wullschleger* [1993]
N g m^{-2}	2.17 ± 0.8	1.74 ± 0.71	3.10 ± 1.35	1.81 ± 0.64	1.86 ± 0.84	1.62 ± 0.61	1.69 ± 0.69	*Kattge et al.* [2009]
χ_n m^2 g^{-1}	0.48	0.59	0.33	0.56	0.57	0.62	0.60	*Kattge et al.* [2009]
Slope (m)	8	8	8	8	8	4	8	*Ball* [1988]; *Leuning* [1995]; *Medlyn et al.* [1999a, 1999b]
Intercept (b), mol m^{-2} s^{-1}	0.0011	0.0011	0.0011	0.0011	0.0011	0.0011	0.0011	*Ball* [1988]; *Leuning* [1995]; *Medlyn et al.* [1999a, 1999b]
LAI	4.07 ± 2.02	3.14 ± 1.99	3.05 ± 1.62	2.42 ± 1.45	1.49 ± 1.06	1.55 ± 1.22	1.64 ± 1.15	*Deng et al.* [2006]
Clumping Index	0.66 ± 0.045	0.70 ± 0.047	0.74 ± 0.057	0.78 ± 0.051	0.75 ± 0.059	0.75 ± 0.050	0.76 ± 0.059	*Chen et al.* [2005]

[a]Where V_{cmax} is the leaf maximum carboxylation rate at 25°C, J_{max} is the maximum electron transport rate, N is the leaf nitrogen content, χ_n is the slope of V_{cmax} variation with N, and m and b are the slope and intercept in the Ball-Berry equation. The peak growing season LAI and clumping index are given as the mean and standard deviation for each plant functional type.

leaf formulation has two serious drawbacks [*Chen et al.*, 1999]. First, the influence of radiation on photosynthesis is lacking in big-leaf models during the growing season. Even under overcast conditions, sky radiation is still nearly sufficient for a big-leaf canopy at proxy, while in reality, shaded leaves or bottom leaves are much less exposed to sky radiation than top leaves and often have insufficient light for photosynthesis. In the big-leaf formulation, the light-limited photosynthesis rate is almost always larger than the nutrient-limited rate, practically diminishing the radiation control over photosynthesis, while in reality radiation is often the main limitation to photosynthesis of shaded leaves in the canopy. Second, big-leaf models assume that photosynthesis takes place in one leaf (or conceptually one layer of leaves), while in reality several layers of leaves operate simultaneously. This assumption dramatically distorts the carbon flow path. In the big-leaf formulation, only one leaf internal resistance operates against the flow of CO_2 from the stomatal cavity (represented by C_i) to the photosynthetic apparatus (represented by the compensation point Γ), and the use of canopy resistance rather than the stomatal resistance only modifies part of the pathway to consider the fact that the carbon flow would meet less resistance through multiple stomatal openings. This description of the flow pathway is quite different from that for multiple layers of leaves that are operating simultaneously, where several internal leaf resistances operate in parallel, as they occur in reality. The two-leaf model used in this study avoids these drawbacks and is effective in investigating the role of shaded leaves in the canopy level photosynthesis, which is altered considerably by canopy architecture.

2.3. Soil Water Influence on Stomatal Conductance

[12] For global GPP modeling, we changed our stomatal conductance scheme from the multiple environmental factor scaling method [*Jarvis*, 1976] to the Ball-Berry formulation shown in equation (4). The reason is that we do not have enough empirical data to establish various scaling functions used in Jarvis' method for the various PTFs. The Ball-Berry formulation provides stable outcomes of the computed stomatal g and A under given meteorological and vegetation structural conditions. However, the important influences of soil water on g and A are not mechanistically included in the original Ball-Berry formulation (equation (4)). Following *Ju et al.* [2006], we modify it as follows:

$$g = f_w\left(m\frac{Ah_s}{C_s}p + b\right) \tag{5}$$

where f_w is a soil moisture scaling factor. The root water uptake modeling scheme developed by *Ju et al.* [2006] is used to calculate f_w in this study. In this scheme, the rate of root water uptake is directly proportional to the soil water availability to the roots. The soil water availability factor $f_{w,i}$ in layer i is calculated as:

$$f_{w,i} = \frac{1.0}{f_i(\psi_i)f_i(T_{s,i})} \tag{6}$$

where $f_i(\psi_i)$ is a function of matrix suction ψ_i(m) [*Zierl*, 2001]. Through simulating tower flux data, we adjusted

constants in *Zierl*'s [2001] function depending on the plant functional type.

[13] For broadleaf evergreen forest:

$$f_i(\psi_i) = \begin{cases} 0.7 + 0.7\left[\dfrac{\psi_i - 10.0}{10.0}\right]^{1.5} & \psi_i > 10 \\ 0.7 & else \end{cases} \quad (7)$$

For broadleaf deciduous and evergreen and deciduous conifer forests:

$$f_i(\psi_i) = \begin{cases} 1.0 + \left[\dfrac{\psi_i - 10.0}{10.0}\right]^{1.5} & \psi_i > 10 \\ 1.0 & else \end{cases} \quad (8)$$

For other four plant functional types:

$$f_i(\psi_i) = \begin{cases} 1.0 + \left[\dfrac{\psi_i - 33.0}{33.0}\right]^{0.4} & \psi_i > 33 \\ 1.0 & else \end{cases} \quad (9)$$

This function increases with increasing matrix suction in the soil, resulting in less soil water available to roots (decreasing $f_{w,i}$). The exponent for forest types in equations (7)–(9) is larger than that for other vegetation types in equation (9) because of their long soil-plant-atmosphere continuum [*Williams et al.*, 1996]. The effect of soil temperature on soil water uptake is described as follows [*Bonan*, 1991]:

$$f_i(T_{s,i}) = \begin{cases} \dfrac{1.0}{1 - \exp\left(t_1 T_{s,i}^{t_2}\right)} & T_{s,i} > 0^\circ C \\ \infty & else \end{cases} \quad (10)$$

where t_1 and t_2 are two parameters determining the sensitivity of water uptake by roots to soil temperature. In this study, $t_1 = 0.02$ and $t_2 = 2.0$.

[14] To consider the variable soil water potential at different depths, we follow the scheme of *Ju et al.* [2006] to calculate the weight of each layer to f_w:

$$w_i = \frac{R_i f_{w,i}}{\sum_{i=1}^{n} R_i f_{w,i}} \quad (11)$$

where R_i is the root fraction in layer i. The overall soil water availability f_w of the whole soil profile is then:

$$f_w = \sum_{i=1}^{n} f_{w,i} w_i \quad (12)$$

The main purpose of equations (11) and (12) is to allow vegetation to optimize the use of its energy by extracting water preferentially from soil layers that require the lowest levels of energy [*Radcliffe et al.*, 1980]. The combination of root distribution and soil water availability in calculating this water stress factor is important in simulating the root water uptake, soil water content, and energy and carbon fluxes [*Li et al.*, 2001; *Prihodko et al.*, 2005].

[15] This scaling factor is based on the physics of soil water potential and its influence on the water flow from roots to leaves. However, the coefficients are empirical and have considerable effects on f_w and the global GPP estimation. Validation of the final GPP modeling results with ground measured GPP is therefore critical in improving the overall accuracy of the modeled global GPP values and its distribution.

3. Input Data

[16] Input data for our global GPP modeling include gridded meteorological data, global land cover map, global LAI maps, and a global clumping index map. The data sources and their processing methodologies are described as follows.

3.1. Gridded Meteorological Data

[17] The original meteorological data, including incoming shortwave radiation, air temperature, specific humidity, precipitation and wind speed, are from the National Center of Environmental Prediction (NCEP) of USA. For hourly modeling at 1° resolution, spatial and temporal interpolations were made to the 6 hourly NCEP data. Spatially NCEP data with the T62 Gaussian grid were linearly interpolated into 1 × 1 degree grids. To interpolate NCEP reanalysis data temporally from 6 hourly to 1 hourly, different methodologies were used for different variables. Hourly values of specific humidity and wind speed were taken the same as NCEP 6 hourly values for each 6 h period. Hourly values of precipitation were simply taken as one-sixth of NCEP 6 hourly values. Hourly radiation was calculated as a function of solar zenith angle for each hour based on daily total radiation from NCEP. The bias in NCEP radiation data is corrected using an equation suggested by *Hicke* [2005]. The average bias is +16%, larger at higher latitudes. Hourly temperature was determined with 6 hourly values and maximum/minimum values in NCEP data, assuming that the maximum temperature happens at local solar time 2:00 p.m. and minimum at 2:00 a.m. NCEP data also have considerable errors in precipitation and temperature [*Zhao et al.*, 2006] that would also have effects on GPP estimated in this study. As these errors are mostly random rather than systematic, they are not yet corrected.

3.2. Global Land Cover Map

[18] Globally, the land cover map in 2000 at 1 km resolution is the GLC2000 (http://www.eogeo.org/GLC2000) produced by individual countries using the SPOT4 VEGETATION data. For the purpose of global GPP modeling, the detailed land cover types are aggregated to six plant functional types (PFT), including broadleaf evergreen forest, broadleaf deciduous forest, evergreen conifer forest, deciduous conifer forest, shrub, and others (mostly crops and grass). For each 1 degree modeling grid, the areal fractions of these PFTs are computed to upscale from 1 km to 1 degree resolution. The C4 vegetation distribution map of *Still et al.* [2003] is used to separate the areal fraction of others into C4 and C3 types in each 1 degree grid. This results in seven functional types in total. We assume that this global land cover map in 2000 is still reliable for our modeling of GPP in 2003.

3.3. Global LAI Maps

[19] The LAI maps in 2003 were produced with cloud-free 10-day synthesis VEGETATION images. These images are

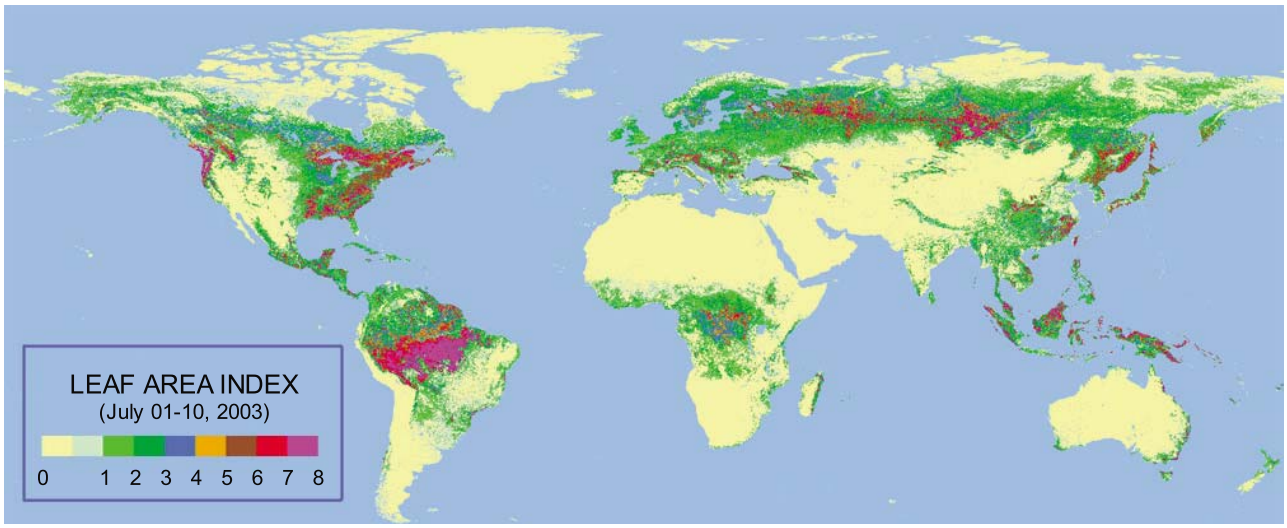

Figure 1. An example of a global leaf area index map in July 1–10 derived from VEGETATION data at 1 km resolution.

atmospherically corrected by the European Space Agency before they are distributed, and reflectances in red, near-infrared (NIR), and mid-infrared (MIR) are used for LAI retrieval using the algorithm developed by *Deng et al.* [2006]. This algorithm, developed based on the 4-Scale geometrical optical model [*Chen and Leblanc*, 1997, 2001], makes use of not only the reflectances but also the angular information at the time of data acquisition for each pixel, including solar zenith angle, view zenith angle, and the difference between sun and satellite azimuth angles. In this way, the variations of the reflectances in the various bands with the angles of sun and satellite, i.e., the bidirectional reflectance distribution functions, are considered. The main characteristics of this algorithm include: (1) the effective LAI is first retrieved based on the reflectances, and a clumping index map (see section 3.4) is used to convert the effective LAI to LAI; and (2) the MIR reflectance is used for forests in order to improve the sensitivity of the algorithm to forest LAI (leaves absorb strongly in MIR) but not used for crops where irrigation might affect MIR. In our remote sensing algorithm, the non-green woody contribution is not included in the effective LAI, and the clumping index includes all scales of clumping. The conversion from effective LAI to LAI is simply: LAI = effective LAI/clumping index, without involving the woody-to-total area ratio and the shoot-to-needle area ratio (in the case of conifer) [*Deng et al.*, 2006].

[20] For reliable terrestrial applications of these LAI images, the residual cloud and atmospheric effects in the LAI images are detected and removed using a Locally Adjusted Cubic-spline Capping (LACC) method based on the seasonal trajectory of each pixel [*Chen et al.*, 2006]. This LAI algorithm has been validated using data from Canada [*Pisek et al.*, 2007] and USA [*Pisek and Chen*, 2007] and also evaluated against MODIS LAI products in these studies. An example of the global LAI map at 1 km resolution for July 1–10, 2003, is shown in Figure 1. The mean of the peak growing season LAI and its standard deviation for each PFT are provided in Table 1.

[21] For GPP modeling at 1°resolution, the LAI images at 1 km resolution are aggregated to obtain the mean LAI values for the six PFTs (section 3.2). This allows for separate GPP calculation for each PFT in each grid. The GPP for each grid cell is then obtained as the sum of GPP for each PFT multiplied by its areal fraction. In the study of *B. Chen et al.* [2007], it is demonstrated that this way of upscaling to a large grid cell can minimize the nonlinear effects of LAI on photosynthesis and is more accurate than the estimation of GPP using the mean LAI for the grid cell for the dominant cover type.

3.4. Global Clumping Index Map

[22] The clumping index of a vegetation canopy can be measured on the ground using an optical instrument named TRAC [*Chen and Cihlar*, 1995], developed based on the canopy gap size distribution theory [*Miller and Norman*, 1971a, 1971b]. TRAC measurements for various cover types show distinct ranges of values and correlate well with an angular index obtained from an airborne sensor POLDER [*Lacaze et al.*, 2002]. An improved angular index, named Normalized Difference between Hot spot and Darkspot (NDHD) was proposed for retrieving the clumping index using multiple angle remote sensing data [*Leblanc et al.*, 2005a; *Chen et al.*, 2005]. The physical principle underlying the derivation of NDHD is that well structured canopies, consisting of foliage clumps at various levels such as shoots, branches and tree crowns, usually cause large variations in reflectance from the hot spot, where the sun and view angles coincide, to the darkspot, where shadows of these clumps are maximally observed. The more clumped is a canopy, the more shadow it has, and hence the darker is the darkspot. The relative variation from the hot spot to the darkspot minimizes the influence of the leaf optical property and accentuates the canopy structural effect.

[23] Through geometric-optical modeling using 4-Scale, linear relationships between the clumping index and NDHD were derived, and these relationships were first used to derive a global clumping index map using POLDER I data at 6 km resolution [*Chen et al.*, 2005]. The POLDER sensor

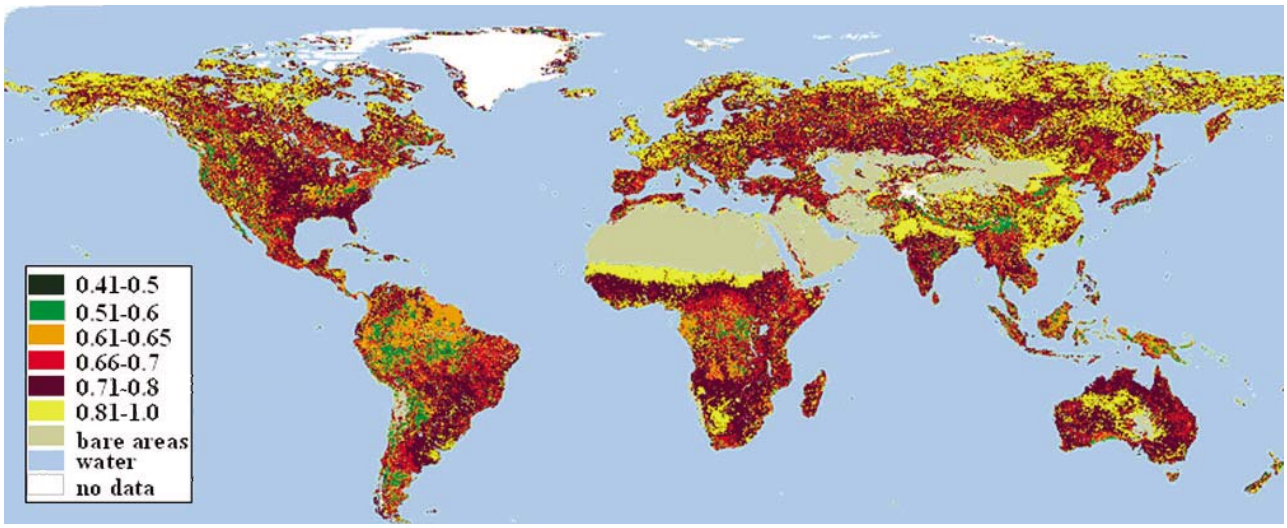

Figure 2. Global clumping index map derived from mostly POLDER III at 6 km resolution.

uses the imaging array technology that allows for data acquisition for a ground target at up to 14 angles during one overpass, and these multiangle observations are accumulated monthly in order to obtain a sufficient cloud-free coverage of the view angle range to retrieve the hot spot and darkspot for each pixel. As POLDER I was short-lived from 30 October 1995 to 30 June 1996, the clumping index map shown in work by *Chen et al.* [2005] has many pixels with missing values because of clouds. We have processed POLDER III data for a full year of 2005, and produced an updated clumping index map (Figure 2). In tropical areas, frequent clouds made it difficult to acquire reliable data for some pixels, and measurements of POLDER I and II are used to supplement the map. This map shows distinct clumping distribution patterns at the global scale. For areas with continuous time series, the temporal variation of the clumping index within the growing season is found to be small relative to measurement noise, and therefore only the seasonal mean value is used in this study. Forested areas generally have low clumping index values (high clumping) while agricultural and grassland have high clumping index values. We realized that 6 km resolution is too coarse to capture the true variability of vegetation structure on the ground, as heterogeneity of the surface due to cover type variation or ground objects with variable heights can also produce shadows and influence the satellite measurements of NDHD. Topographical shadows would also increase NDHD and therefore cause considerable negative biases on the vegetation clumping retrieval. In this new clumping map, the first order effects of topographical variation has been removed based on the standard deviation of the digital elevation model at 1 km resolution within each 6 km pixel [*Pisek et al.*, 2010].

[24] This clumping map is the basis for our evaluation of the importance of 3-dimensional canopy structure in global GPP estimation. As the resolution is low (6 km), it is currently not feasible to validate this map. However, we have conducted a preliminary evaluation of the map using existing ground-based measurements using TRAC reported in the literature. There are 39 data points collected in forests, woodlands and savannas in Canada, USA, China, Japan, Zambia, Botswana, Israel, Belgium, Estonia, and Czech Republic, and the majority of them were taken in forest stands. When a simple comparison between a ground point and a 6 × 6 km pixel was made for all points, the mean bias error (MBE) was 0.104. However, when we select data points that match with the dominant cover type in the clumping map, the MBE becomes 0.027 for woodlands and savannas (7 sites) and 0.046 for forest stands (17 sites) [*Pisek et al.*, 2010]. These small errors give us some confidence in the clumping map. The mean and standard deviation of the clumping index for each PFT are provided in Table 1. The mean values for C4 and other vegetation (including crops and grass) seem to be smaller than their expected typical values [*Chen et al.*, 2005]. This may be due to shadowing effects on NDHD caused by surface heterogeneity rather than stand structure, indicating a limitation of this coarse resolution data set. In addition to clouds in tropical areas, aerosols from biomass burning would also influence the surface reflectance measurements. However, as NDHD is based on the ratio of the hot spot and darkspot, the error caused by aerosols is greatly minimized. Field-measured clumping index values are shown to have significant variations with solar zenith angle [*Chen*, 1996b; *Leblanc et al.*, 2005b] and season [*Ryu et al.*, 2010b]. However, only a fix clumping index value is used per pixel because we don't yet have sufficient knowledge of its diurnal and seasonal variation patterns.

3.5. Global Soil Texture Map

[25] Soil texture for each 1 × 1 degree grid was determined based on the fractions of clay, silt and sand in soil. The data were obtained from NASA [*Webb et al.*, 1991]. They are used to estimate hydrological parameters, including porosity, field capacity (water potential at 33 kPa), wilting point (water potential at 1500 kPa), saturated hydraulic conductivity, and air entry water potential [*Saxton et al.*, 1986; *Campbell and Norman*, 1998]. These parameters

were used to calculate the water holding capacity and the soil water scaling parameter f_w (section 2.3).

4. Modeling Cases and Model Validation

[26] For the purpose of investigating the impact of foliage clumping on the global GPP estimation, we conduct model simulations for the following three cases:

[27] 1. Case I: The clumping index is considered in both LAI retrieval and in GPP modeling. In this case, the effective LAI retrieved from remote sensing is converted to LAI using the clumping index map. This converted LAI is assumed to represent the true LAI. The clumping index map is also used in sunlit and shaded leaf separation (equations (2a) and (2b)). This case is considered to be unbiased and representative of the reality.

[28] 2. Case II: The same true LAI as in Case I is used, but the clumping is ignored, i.e., clumping index = 1 is assumed. This is the case that the true LAI is available (such as those obtained through destructive sampling or using allometric equations) but a random leaf spatial distribution is assumed. In this case, the sunlit leaf area is overestimated and the shaded leaf area is underestimated as compared with Case I.

[29] 3. Case III: Only the effective LAI (L_e) retrieved from remote sensing is used and the clumping index is taken as unity (i.e., ΩL in equation (2a) is replaced by L_e). In this case, the sunlit leaf area is the same as Case I, but the shaded leaf area is underestimated.

[30] By comparing Case II to Case I, we demonstrate the importance in considering clumping when the true LAI is available. By comparing Case III to Case I, we demonstrate the importance in considering clumping when LAI is derived indirectly from remote sensing images. Case III may be particularly relevant to global GPP estimation as the essential signal from optical remote sensing at one angle is the canopy gap fraction (or the percent canopy cover) at that angle, which is then converted to the effective LAI, while the true LAI is unknown. Some global and regional LAI products in previous intercomparison studies [*Morisette et al.*, 2006; *Garrigues et al.*, 2008] are in fact effective LAI products. Although several products have considered the clumping effect to some extent, the consideration is often incomplete, causing largest differences among different LAI products for most clumped canopies [*Garrigues et al.*, 2008]. The effective LAI derived from remote sensing is often conveniently assumed to be the true LAI, causing underestimation of the shaded LAI, while the sunlit LAI is unaffected by this assumption. As the sunlit leaves have higher productivity than shaded leaves, we may tend to think that this assumption is reasonable and may not cause considerable errors in the global GPP estimation. One of the main purposes of this study is to evaluate the impact of this assumption.

[31] The BEPS model has been validated extensively with GPP data derived from eddy-covariance (EC) measurements for boreal and temperate ecosystems in Canada and USA [*Ju et al.*, 2006; *Chen et al.*, 2008] and for tree ring-derived NPP for temperate and semi-arid ecosystems in China [*X. Chen et al.*, 2007; *Wang et al.*, 2007; *Zhou et al.*, 2007; *Zheng et al.*, 2007]. Hourly GPP modeled by BEPS is recently compared against EC measurements 11 sites in North America, with r^2 ranging from 0.71 to 0.92 for 10 sites and equal to 0.32 for 1 site. The modeled annual total GPP differs from EC-derived GPP by less than 10% at each of these 11 sites [*Sprintsin et al.*, 2012]. Based on data in work by *Huete et al.* [2006] and *Saigusa et al.* [2008], our modeled GPP values in 2003 were 2914 and 3482 gC $m^{-2}y^{-1}$ for two tropical rain forests, KM67 (2.86°N, 54.96°W) in Brazil and Sakaerat (14.5°N, 101.9°E) in Thailand, respectively, as compared with EC-derived values of 3105 and 3930 gC $m^{-2}y^{-1}$, respectively. The accuracy of the LAI values for these stands is the major uncertainty for our model validation for tropical forests. Considerable uncertainties exist in the global GPP simulated by BEPS, and a set of sensitivity tests are made to assess these uncertainties and discussed in section 6.

5. Results

[32] Using the various vegetation, soil and meteorology inputs, a global GPP map is computed at one degree resolution in hourly time steps for 2003 for each of the three cases. The resulting global GPP map for Case I, the ideal case representing the reality in our study, is shown in Figure 3. The global GPP value is 132 ± 22 PgC y^{-1}, where the uncertainty ± 22 PgC y^{-1} is the sum of the uncertainty (± 21 PgC y^{-1}) caused by the input vegetation data and model parameters and the standard deviation (± 1 PgC y^{-1}, Table 2) of the annual global GPP over the period from 2000 to 2007 caused by meteorological variations. The uncertainty caused by input data and model parameters is approximated by the range of global GPP variation caused by LAI uncertainty of 20% (see section 6 and Table 3). Although uncertainties caused by other parameters would be additive to the uncertainty caused by LAI in the error theory if other parameters are independent of LAI, it is reasonable to use the uncertainty caused by LAI to represent the total uncertainty because other parameters (such as clumping index) could be correlated with LAI to some extent and also because in the calibration of BEPS against tower flux and other data, many model parameters are fine-tuned with given LAI values (measured with errors of about 15%) and the effects of the errors of model parameters on modeled GPP are generally absorbed into the uncertainty caused by the error in measured LAI. The standard deviation in annual global GPP caused by meteorological variations is much smaller than the uncertainty caused by LAI. It is obtained using the same model parameters and the same seasonal LAI variation in 2003 but actual hourly meteorological data from 2000 to 2007. This standard deviation in GPP is similar to the standard deviation of 0.8 PgC y^{-1} in NPP or about 1.6 PgC y^{-1} in GPP from 1990 to 2001 [*Piao et al.*, 2009], which includes both meteorological and ecosystem variations.

[33] The GPP distribution pattern shown in this map broadly resembles those of *Alton et al.* [2007] and *Beer et al.* [2010]. When it is scaled to NPP, the distribution pattern is also similar to those of *Cramer et al.* [1999], *Goetz et al.* [2000], and *Krinner et al.* [2005]. However, our results tend to show higher GPP or NPP values for the tropical areas than most existing results. We obtain larger GPP values for tropical forests mostly due to leaf clumping in these forests as shown in the global clumping index map (Figure 2). In the study by *Chen et al.* [2005], reflectances from tropical

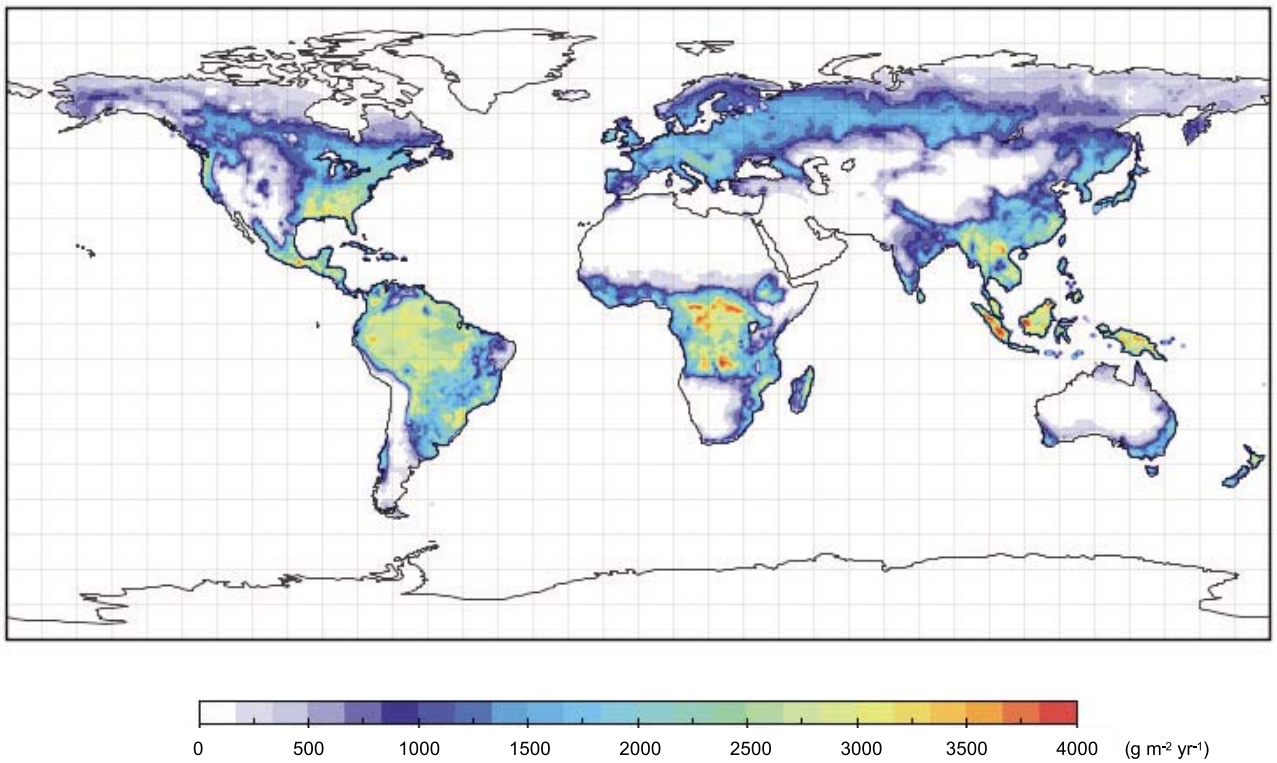

Figure 3. Global GPP map in 2003 (Case I, i.e., the ideal case), calculated with consideration of foliage clumping (Figure 2).

forests were found to vary pronouncedly with view angles due to their multilayered structure and large tree crowns at the top layer casting large shadows. This shadowing effect is captured in the multiangle remote sensing images and is taken as the indication of foliage clumping. In other words, the use of the clumping index would more or less correctly compensate for the amount of shaded leaf area which would otherwise have been underestimated if the canopy were assumed to be random. As few of the models (including ours) used for global GPP or NPP mapping have been intensively validated using reliable site level data in productive rain forests, the estimation of GPP for tropical rain forests remains error prone and further improvement is yet to be made. We have also found no ground-based clumping measurements reported in the literature and therefore would like to encourage this parameter to be measured at various heights to address the issue of different clumping levels of the different layers of vegetation.

[34] On the basis of Case I, the effect of foliage clumping on global GPP estimation is evaluated. Figure 4 shows the

Table 2. Sunlit and Shaded Leaf GPP and the Total GPP (Pg C y^{-1}) for the Various Plant Functional Types (PTFs) Under Three Canopy Architectural Treatments[a]

PTF		Broadleaf Evergreen	Broadleaf Deciduous	Evergreen Conifers	Deciduous Conifers	Shrub	C4 Plants	Others	Total
Sunlit GPP	Case I	15.80 ± 0.02	19.20 ± 0.08	9.18 ± 0.11	1.22 ± 0.04	7.98 ± 0.04	3.06 ± 0.01	29.49 ± 0.12	85.94 ± 0.38
	Case II	19.13 ± 0.03	22.88 ± 0.10	10.72 ± 0.12	1.38 ± 0.05	9.85 ± 0.05	3.82 ± 0.02	36.21 ± 0.15	103.99 ± 0.52
	Case III	16.19 ± 0.03	20.84 ± 0.11	9.86 ± 0.11	1.29 ± 0.04	8.28 ± 0.04	3.24 ± 0.02	30.99 ± 0.12	90.69 ± 0.41
Shaded GPP	Case I	15.96 ± 0.23	11.52 ± 0.20	5.42 ± 0.09	0.78 ± 0.01	2.74 ± 0.02	1.25 ± 0.01	8.02 ± 0.14	45.67 ± 0.76
	Case II	15.81 ± 0.08	11.06 ± 0.06	5.23 ± 0.05	0.75 ± 0.01	2.42 ± 0.05	1.06 ± 0.05	7.16 ± 0.03	43.50 ± 0.24
	Case III	11.20 ± 0.06	7.47 ± 0.05	3.60 ± 0.04	0.55 ± 0.01	1.54 ± 0.04	0.57 ± 0.01	3.90 ± 0.02	28.83 ± 0.19
Total GPP	Case I	31.76 ± 0.26	30.72 ± 0.24	14.60 ± 0.16	2.00 ± 0.05	10.72 ± 0.05	4.31 ± 0.02	37.51 ± 0.22	131.61 ± 0.96
	Case II	34.94 ± 0.11	33.94 ± 0.14	15.95 ± 0.15	2.13 ± 0.05	12.27 ± 0.06	4.88 ± 0.02	43.37 ± 0.15	147.49 ± 0.62
	Case III	29.39 ± 0.09	28.31 ± 0.12	13.46 ± 0.12	1.84 ± 0.04	9.82 ± 0.05	3.81 ± 0.02	34.89 ± 0.14	121.52 ± 0.54
Case II − Case I		3.18 ± 0.35	3.22 ± 0.29	1.35 ± 0.14	0.13 ± 0.01	1.55 ± 0.06	0.57 ± 0.02	5.86 ± 0.19	15.88 ± 0.96
Case III − Case I		−4.37 ± 0.10	−2.41 ± 0.11	−1.14 ± 0.11	−0.16 ± 0.12	−0.90 ± 0.03	−0.50 ± 0.01	−2.62 ± 0.15	−12.09 ± 0.54

[a](1) LAI is accurate and clumping is considered (Case I); (2) LAI is accurate but clumping is ignored, i.e., clumping index = 1 under the assumption of random leaf spatial distribution (Case II); and (3) the effective LAI is available and no clumping is considered (Case III). The uncertainty range is the standard deviation of the annual GPP for the period from 2000 to 2007 for each PFT and each case. (The total uncertainty is this uncertainty plus that due to 20% LAI error, see Table 3.) Based on double-tailed *t* tests, the differences between Case I and Case II and between Case I and Case III for each PTF and the global total GPP are all statistically highly significant ($p < 0.001$) against the interannual variation of GPP.

Table 3. Sensitivities of Global GPP (Pg C y^{-1}) to Errors in the Major Input Parameters of LAI and Clumping Index (Ω) as Well as the Most Uncertain Soil Water Scalar (f_w) for Stomatal Conductance (Equations (6)–(12))

	Case I	Case II	Case III	Case II – Case I[a]	Case III – Case I[a]
Baseline[b]	131.61	147.48	121.51	15.87 (12.1%)	−10.10 (7.7%)
1.2 * LAI	144.68	161.01	135.31	16.33 (11.3%)	−9.37 (6.5%)
0.8 * LAI	115.69	130.97	106.3	15.28 (13.2%)	−9.39 (8.1%)
1.2 * f_w	134.56	150.97	124.49	16.41 (12.2%)	−10.07 (7.5%)
0.8 * f_w	127.15	142.16	116.93	15.01 (11.8%)	−10.22 (8.0%)
1.2 * Ω	139.95	151.28	130.20	11.33 (8.1%)	−9.75 (7.0%)
0.8 * Ω	121.94	137.1	111.61	15.16 (12.4%)	−10.33 (8.5%)
1.2 * *V*cmax	147.58	160.83	127.01	13.25 (9.0%)	−20.57 (−13.9%)
0.8 * *V*cmax	113.00	121.93	94.50	8.93 (7.9%)	−18.50 (−16.4%)

[a]The percentage in the brackets in the last two columns is the difference relative to Case I.
[b]The baseline represents the ideal case shown in Table 2 and Figure 4.

total GPP values for each PFT for the three cases. GPP values for Case II are always higher than the corresponding values for Case I. This is because the sunlit LAI is overestimated in Case II in which the correct LAI is used without considering the clumping effect. In reality, foliage clumping increases the light penetration through the canopy and reduces the sunlit LAI, although in the meantime it increases the shaded LAI. When this clumping effect is ignored, sunlit LAI is overestimated and shaded LAI is underestimated. As sunlit GPP is larger than shaded GPP per unit leaf area, the total GPP is overestimated in Case II (Table 2). Opposite to Case II, ignoring clumping in Case III results in underestimation of GPP. This is because the effective LAI is much smaller than the true LAI for a clumped canopy. When the effective LAI is used without considering clumping, the sunlit LAI is the same as that in Case I, but the shaded LAI is much smaller than that in Case I. The shaded GPP values in Case III are therefore smaller than those in Case I for the various PFTs (Table 2). There are slight differences in sunlit GPP between Case I and Case III because clumping has a slight effect of the diffuse irradiance on sunlit leaves due to multiple scattering [*Chen et al.*, 1999].

[35] Through the conventional two-tailed *t* test, the significance of the clumping effect is assessed against the GPP interannual standard deviation. The differences in GPP between Case I and Case II and between Case I and Case III for the individual PFTs (Table 2) are all statistically significant at $p < 0.001$, meaning that the clumping effect for either Case II or Case III is highly significant relative to the combined effect of the interannual variations in meteorological conditions. Another way of assessing the statistical significance of the clumping effect is shown in Figures 5 and 6. The overall difference in GPP is +15.88 PgC y^{-1} (12.0%) between Case II and Case I and −12.09 PgC y^{-1} (9.2%) between Case III and Case I. GPP in Case III is negatively biased to a considerable extent because of the large contributions of shaded leaves to the total canopy GPP. The fraction of the shaded to total GPP is 50%, 38%, 37%, 39%, 26%, 29% and 21% to the total GPP for broadleaf evergreen forest, broadleaf deciduous forest, evergreen conifer forest, deciduous conifer forest, shrub, C4 vegetation, and other vegetation, respectively (Table 2, for Case I). The difference in the total GPP between Case I and Case II is larger than that between Case I and Case III

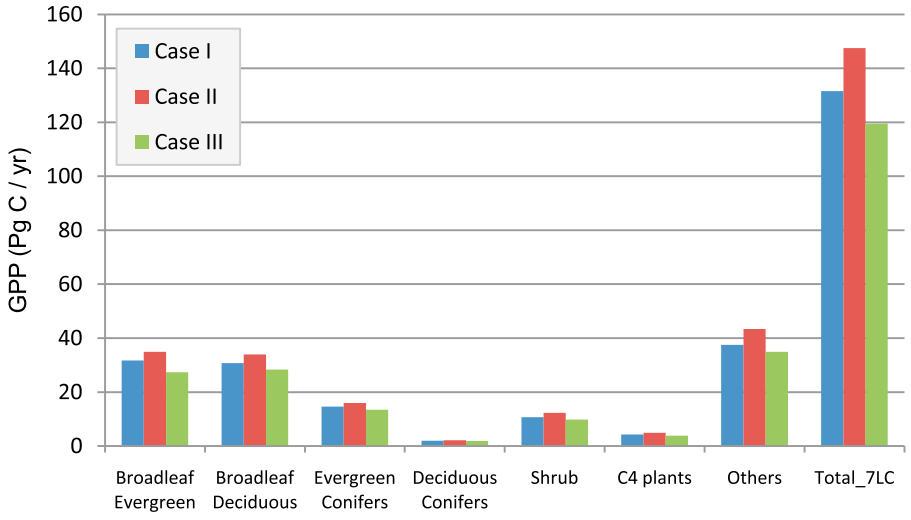

Figure 4. The effect of foliage clumping on GPP of the various plant functional types. Case I: the LAI is accurate and clumping is considered (representing the reality); Case II: the LAI is accurate but the clumping is ignored; and Case III: the effective LAI is available and no clumping is considered.

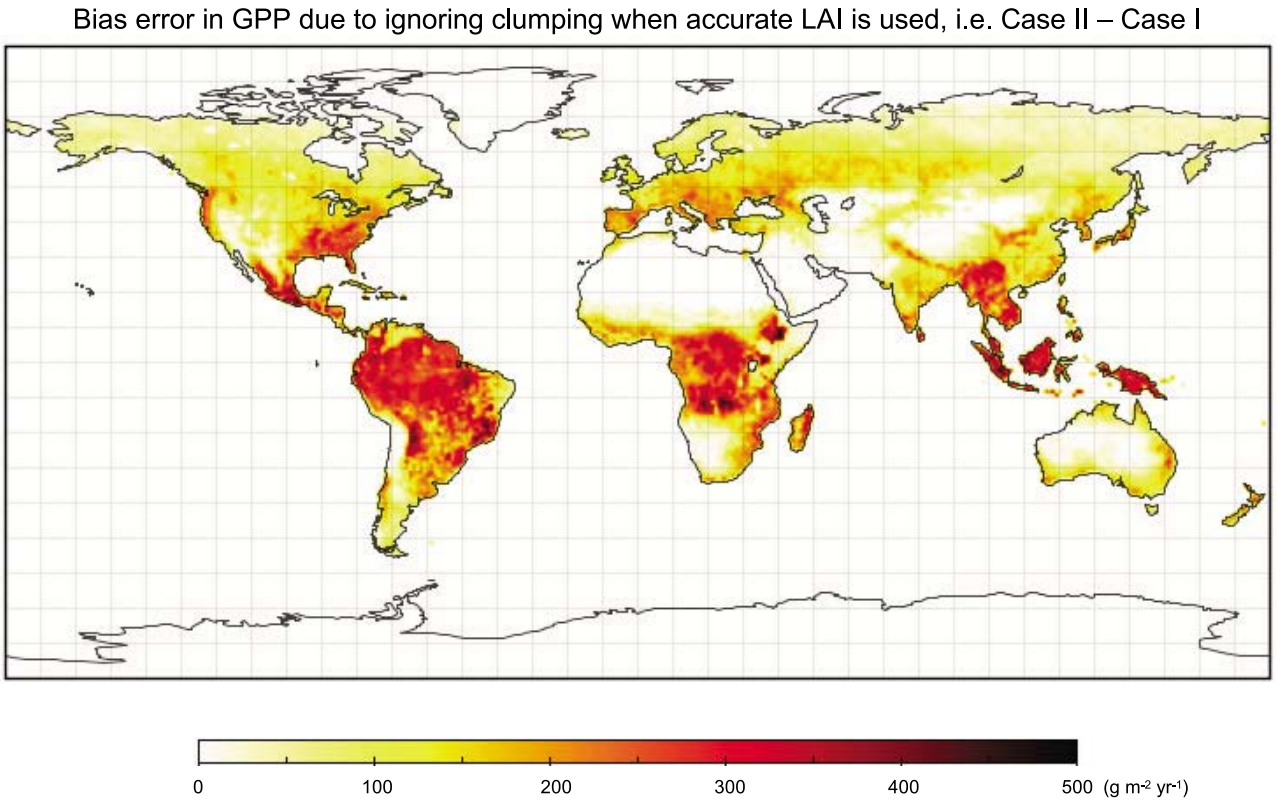

Figure 5. GPP estimates are positively biased when accurate LAI is available but clumping is ignored. Case I: the LAI is accurate and clumping is considered, and Case II: the LAI is accurate but the clumping is ignored. The global average positive bias (Case I − Case II) is 15.88 PgC y^{-1}, which is 12% of the global GPP.

because GPP is more sensitive to the overestimation of sunlit LAI than to the underestimation of shaded LAI. *Alton et al.* [2007] claimed that foliage clumping affects global GPP by less than 5% when they effectively examined the difference between Case I and Case II through the use of a 3-dimensional canopy radiative transfer model which presumably uses the true LAI rather than effective LAI. We found that this clumping effect is sensitive to the treatment of the vertical leaf nitrogen gradient in the canopy. The exponential decrease of the leaf nitrogen content assumed in our study (Appendix B) results in V_{cmax} for sunlit leaves being considerably larger than that for shaded leaves, making the canopy-level GPP sensitive to the overestimation of sunlit LAI when clumping is ignored. This may be part of the reason that the clumping effect found in our study is larger than that of *Alton et al.* [2007].

[36] The spatial distributions of the difference in GPP between Case II and Case I and between Case III and Case I display consistent signs of the clumping effects, either positive (Figure 5) or negative (Figure 6), demonstrating that these clumping effects are consistent spatially, in spite of large variations in other factors including vegetation, soil and meteorology. In other words, the clumping effects are important in both cases. Both Figures 5 and 6 illustrate that the largest biases due to ignoring the clumping effect occur in tropical areas where considerable clumping is derived from multiple angle remote sensing (Figure 2). Although the relative effect of clumping is similar among functional types (Table 2), the absolute differences are largest for broadleaf functional types because of their large total GPP values. Figure 5 demonstrates that by ignoring the clumping effect when accurate LAI is available, the GPP value is overestimated in almost all locations of the globe. Figure 6 shows the opposite effect of clumping in all locations of the globe when the effective LAI is used without considering the clumping. In these spatial distribution patterns showing the clumping effect on GPP, the largest uncertainty in terms of the absolute values belongs to the tropical forests as few clumping index values are available for the validation. Shrubs, C4 and other vegetation types would also have considerable errors because the BEPS model has not been extensively validated for these functional types and because the clumping values may be negatively biased due to shadow effects other than the canopy structure on the remote sensing of NDHD [*Chen et al.*, 2005].

[37] It is particularly interesting to note that the detailed spatial variations of the clumping effects shown in Figures 5 and 6 are relatively different. In Case II (Figure 5), the largest clumping effects on GPP do not occur where the LAI is largest. This is because the relative change in the amount of shaded LAI with clumping is larger at lower LAI values, while the absolute amount of shaded LAI changes little with LAI (equations (2a) and (2b)). In Case III (Figure 6), the largest clumping effects occur in areas with the largest LAI.

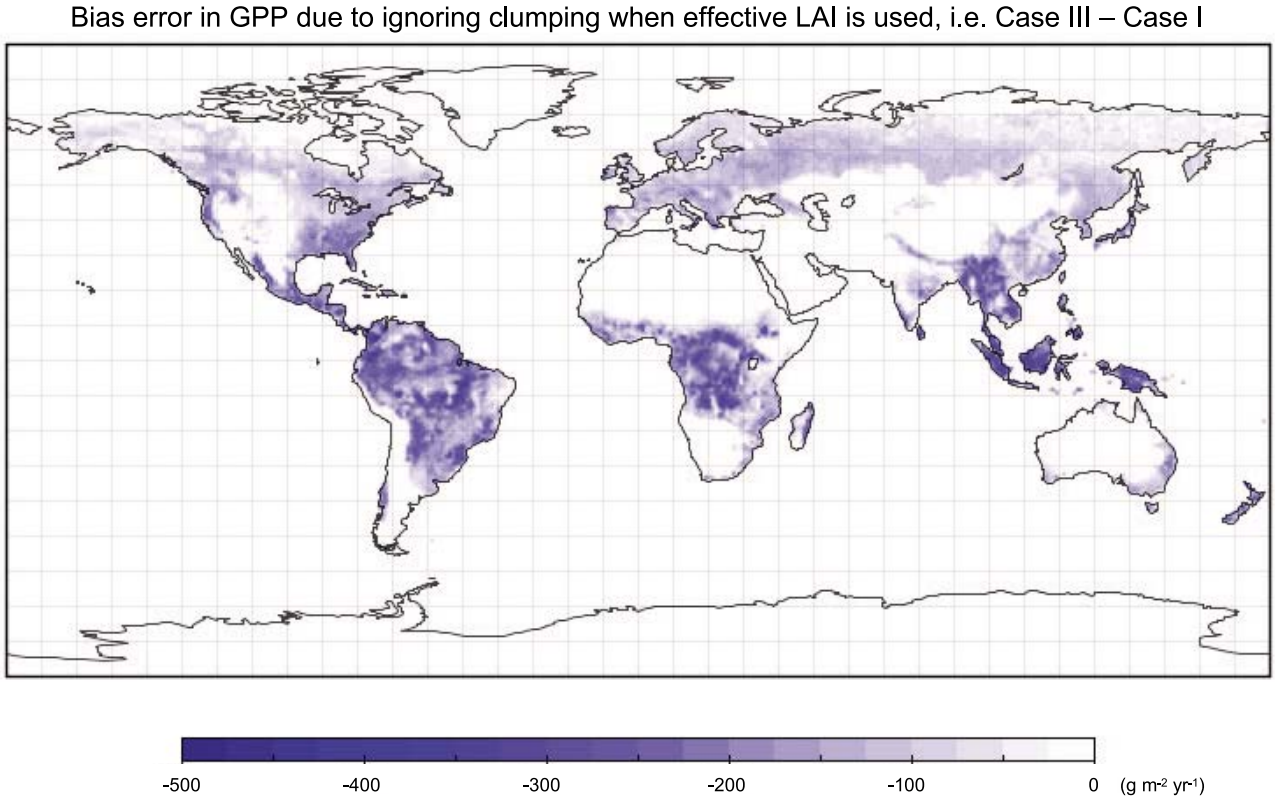

Figure 6. GPP estimates are negatively biased when the effective LAI derived from remote sensing is used without considering clumping. Case I: the LAI is accurate and clumping is considered, and Case III: the effective LAI is available and no clumping is considered. The global average negative bias (Case I − Case III) is –12.09 PgC y^{-1}, which is 9% of the global GPP.

This is because if the clumping index is the same, the shaded LAI is more underestimated with larger LAI values.

6. Discussion

[38] It is obvious that uncertainties in our GPP estimation due to errors in input and model parameters would be as large as the clumping effects reported above. In order to explore the reliability of our conclusion about the clumping effects as shown in Figures 5 and 6, we conducted a set of sensitivity tests and the results are shown in Table 3. When the LAI in each modeling grid is uniformly increased or decreased by 20% (assessed LAI error), the global GPP is increased or decreased by about 11%. However, the relative differences between Case I and Case II and between Case I and Case III change very little (less than 1%) with these LAI changes. This is because a LAI change in one direction would affect all cases in the same direction. Similarly, forcing the soil water scalar (f_w) and V_{cmax} to increase or decrease by 20% in the model would result in increases or decreases in the global GPP in similar magnitudes, while the relative differences between the cases quantifying the clumping effects are affected very little. In general, modifying other parameters in the model, such as J_{max} and m values (Table 1) would move all of the three cases in the same direction, and the clumping effects quantified as the relative differences in GPP would not be much affected by these modifications. This set of sensitivity analysis underpins the reasons for the spatially consistent clumping effects shown in Figures 5 and 6 and supports the levels of their statistical significance.

[39] As expected, increasing or decreasing the clumping index value by 20% changes the relative differences among the cases considerably (Table 3). In our preliminary evaluation using existing ground data, the mean bias error of the clumping map is found to be smaller than 0.05 (6%) (section 3.4), and this 20% change would therefore be generous for most cover types. We have made the range variation large in order to cover the large uncertainty in the clumping estimation for tropical forests. Although the clumping is reduced by 20% (the clumping index is increased), we would still have 8% difference between Case I and Case II and 7% difference between Case I and Case III, suggesting that the influence of clumping cannot be ignored even if there is still considerable uncertainty in its measurement.

[40] For the purpose of GPP estimation, the description of the complex canopy structure requires at least two parameters: the commonly used LAI and the clumping index Both parameters can be obtained from remote sensing. However, their accuracies are still in question. Currently, several LAI products are available using various remote sensing algorithms [*Myneni et al.*, 2002; *Baret et al.*, 2006, 2007; *Deng et al.*, 2006]. Depending on ground data and models used in the algorithm development, some LAI products are close to the effective LAI while some are more or

less close to the true LAI. If the ground data are obtained through destructive sampling or based on allometric equations, the LAI is likely to be close to the true LAI. If the ground data are obtained with optical instruments, such as the LAI-2000 or hemispherical cameras, without making the clumping correction, the LAI is likely to be the effective LAI. Many remote sensing LAI algorithms were developed based on optical measurements on the ground without the clumping correction, and therefore these algorithms produces the effective LAI rather than the true LAI, although some of the recent LAI products have considered the clumping effects in various ways [*Morisette et al.*, 2006; *Garrigues et al.*, 2008]. Although our LAI algorithm [*Deng et al.*, 2006] (GLOBCARBON algorithm in work by *Garrigues et al.* [2008]) has included the clumping effect, the accuracy of the clumping index map used for LAI production is still unsatisfactory. Multiple angle optical remote sensing required for clumping mapping is so far available at very low spatial resolution (6 km). Although other sensors, such as MISR or MODIS, provide multiple angle measurements at 250 m or 275 m resolutions, their view angles are too far from the principle plane to derive the hot spot and darkspot accurately. Remote sensing technology is yet to be further developed to meet the requirement of global terrestrial carbon cycle research.

[41] Many early models use the parameter of the fraction of photosynthetically active radiation absorbed by the canopy (FPAR) [*Potter et al.*, 1993; *Ruimy et al.*, 1996; *Goetz et al.*, 2000; *Running et al.*, 2004]. These models apparently avoid the problems mentioned above associated with the use of LAI. However, it must be realized that FPAR is not an intrinsic canopy structural parameter. It changes with solar zenith angle greatly during a day, and it also differs between sunny and cloudy conditions. The FPAR parameter cannot be used to differentiate between sunlit and shaded leaves, which are biochemically controlled by different processes during photosynthesis. The use of FPAR for GPP or NPP estimation is therefore only a gross first approximation. Although many errors in photosynthesis estimation due to the complex canopy structure can be absorbed into the light use efficiency, the use of cover type specific light use efficiencies cannot capture the spatial and temporal variabilities in GPP or NPP. One way to improve global GPP estimation using process models would be to acquire better description of the canopy architecture in terms of the foliage abundance (LAI) and organizational pattern (clumping). In this study, the possible variation of the clumping index with zenith angle [*Chen*, 1996b; *Leblanc et al.*, 2005b] is ignored, but it can be considered in later studies when this variation can be better quantified through more field measurement.

7. Conclusion

[42] The importance of foliage clumping in its influence on the terrestrial primary productivity is investigated in two ways: (1) through its influence on sunlit and shaded leaf stratification, and (2) through its influence on LAI retrieval from remote sensing. Through global GPP modeling with and without a new global clumping index map, the following conclusions are drawn:

[43] 1. Even if we have an accurate LAI map for the globe, ignoring the foliage clumping effect would result in an overestimation of the global GPP by about 12%. This is because clumping decreases the sunlit LAI and increases the shaded LAI, causing an overall decrease in GPP.

[44] 2. When the effective LAI is obtained from optical remote sensing, ignoring the foliage clumping effect would cause an underestimation of the global GPP by 9%. This is because the effective LAI is much smaller than the true LAI when a canopy is clumped. When the effective LAI is used in GPP modeling without considering the clumping effect, the shaded LAI is considerably underestimated, resulting in the underestimation of GPP.

[45] 3. Even though the uncertainties in the global GPP estimation are large, i.e., the true value of global GPP remains unknown, the clumping effects found as the relative differences between the cases with and without the clumping consideration are still reliable because errors in input and model parameters would move all cases in the same directions.

[46] The underestimation case is particularly relevant to remote sensing because global LAI maps are often generated using algorithms developed with ground data measured with optical instruments without considering the clumping effect. The overestimation case suggests the importance of using the clumping index as the second parameter even if the true LAI is derived. According to this study, we make the following suggestions:

[47] 1. In global GPP modeling, we should use not only LAI but also clumping index. Both parameters are needed in sunlit and shaded LAI calculations and in GPP estimation using two-leaf models. This separate two-leaf estimation is essential as sunlit and shaded leaves are controlled by different biochemical processes during photosynthesis.

[48] 2. To better serve the need of global carbon cycle research, the remote sensing community should produce accurate maps for both clumping index and LAI. Multiple angle remote sensing sensors that are capable of capturing the vegetation structural effect near the principle plane at moderate resolutions (250–1000 m) are still lacking for this purpose.

Appendix A: Sunlit and Shaded Leaf Irradiances

[49] Sunlit and shaded leaf irradiances are important variables for computing sunlit and shaded leaf photosynthesis rates. The input total solar irradiance above the plant canopy (S_g) is first partitioned into direct and diffuse irradiances using an empirical formula of *Erbs et al.* [1982], which was modified and validated by *Black et al.* [1991] for northern environment. The fraction of diffuse radiation in the total is determined by:

$$\frac{S_{dif}}{S_g} = \begin{cases} 0.943 + 0.734R - 4.9R^2 + 1.796R^3 + 2.058R^4 & R < 0.8 \\ 0.13 & R > 0.8 \end{cases} \tag{A1}$$

where S_g is the global solar radiation in W m^{-2}. R is a ratio equal to $S_g/(S_o \cos\theta)$ where S_o is the solar constant (= 1367 W m^{-2}). The direct radiation fraction above the canopy (S_{dir}) is the remainder of the diffuse fraction. This empirical equation is derived based on data obtained under

a midlatitude marine air mass near Vancouver, Canada. The diffuse radiation fraction estimated from this equation is within the variation range of data assembled by *Spitters et al.* [1986] from 9 locations over the globe, but is about 5–10% lower than the mean value across the entire R range. However, this equation would underestimate the diffuse fraction for air masses with large aerosol contents.

[50] With S_{dif} and therefore S_{dir} determined from equation (A1), the sunlit leaf irradiance (S_{sun}) is calculated as [*Norman*, 1982]:

$$S_{sun} = S_{dir}\cos\alpha/\cos\theta + S_{sh} \tag{A2}$$

where α is the mean leaf-sun angle. $\alpha = 60°$ is a good approximation for a canopy with spherical leaf angle distribution [*Chen*, 1996a]. Because S_{dir} is proportional to $\cos\theta$, S_{sun} changes little in a day. With the consideration of the foliage clumping effect, a different method for estimating the mean shaded leaf irradiance (S_{shade}) is developed based on radiative transfer physics. It is summarized as follows:

$$S_{sh} = \frac{(1-\delta)}{L}\left(S_{dif} - S_{dif,under}\right) + C \tag{A3}$$

where $S_{dif,\ under}$ is diffuse radiation under the plant canopy, δ is a correction for nonlinear response of leaf photosynthesis to the vertical variation of diffuse radiation within the canopy (see equation (A7) below), and C represents the additional source of diffuse radiation in the canopy due to multiple scattering of direct radiation [*Norman*, 1982]:

$$C = 0.07\Omega S_{dir}(1.1 - 0.1L)e^{-\cos\theta}. \tag{A4}$$

[51] Equation (A3) states that diffuse irradiance on shaded leaves originates from two sources: sky irradiance and multiple scattering of the incident radiation within the canopy. This term is verified using a geometric-optical model 5-Scale with a multiple scattering scheme [*Chen and Leblanc*, 2001]. The first term in equation (A3) makes the average of the total intercepted diffuse radiation from the sky for the total LAI involved (sunlit leaves also contribute to the interception). The diffuse radiation reaching to the forest floor is calculated using the simple equation with the consideration of the clumping effect (Ω):

$$S_{dif,under} = S_{dif}e^{-0.5\Omega L/\cos\bar{\theta}} \tag{A5}$$

where $\bar{\theta}$ is a representative zenith angle for diffuse radiation transmission and slightly dependent on LAI:

$$\cos\bar{\theta} = 0.537 + 0.025L \tag{A6}$$

This is a simple but an effective way to calculate the transmitted diffuse radiation. It avoids the integration of the sky irradiance for the hemisphere by using a representative transmission zenith angle $\bar{\theta}$, which is obtained through a numerical experiment with the complete integration. Under the assumption of isotropic sky radiance distribution, it is near a constant of 57.5° but also a weak function of LAI. This angle is larger than the mean of 45° because the hemisphere is more heavily weighted against the lower sphere in the integration. The dependence on LAI is found because it modifies slightly the weight distribution.

[52] The nonlinearity correction factor δ is expressed as

$$\delta = 0.2\left(1 - e^{-0.5\Omega L/\cos\bar{\theta}}\right) \tag{A7}$$

This correction is near zero when LAI is small and increases with LAI to a maximum of 0.2. This semi-empirical equation is derived according to the probability of shaded leaves at depth L and the shape of the curve $J = S_{dif}(L)J_{\max}/(S_{dif}(L) + 2.1J_{\max})$ against $S_{dif}(L)$, where $J_{\max}$ is the maximum electron transport rate (Table 1), and $S_{dif}(L)$ is the diffuse irradiance at L. Numerical integration of J weighted by shaded leaf probability is conducted with respect to L, and the results are approximated as equation (A7).

[53] Our methodology for sunlit and shaded leaf irradiance calculation differs substantially from those of *De Pury and Farquhar* [1997] and *Wang and Leuning* [1998]. They calculate the total radiation absorptions by sunlit and shaded leaf groups and treat each group as a big leaf, and therefore their models are two-bigleaf models. Our model aims at obtaining the incident irradiances on representative sunlit and shaded leaves, and in this way the problem of CO_2 flow distortion associated with bigleaf formulation (see section 2.3) is entirely avoided. Through numerical experiments, we have reduced some radiation transfer physics into simple equations suitable for regional and global applications using remote sensing data.

Appendix B: Nitrogen-Weighted V_{cmax} and J_{max} for Sunlit and Shaded Leaves

[54] Leaf nitrogen content per unit leaf area $N(L)$ generally decreases exponentially from the top to the bottom of a canopy [*De Pury and Farquhar*, 1997; *Kattge et al.*, 2009] and can be expressed as:

$$N(L) = N_0 e^{-k_n L} \tag{B1}$$

where N_0 is the nitrogen content at the top of the canopy, and k_n is the leaf nitrogen content decay rate with increasing depth into the canopy, i.e., LAI (L). In this study we assume $k_n = 0.3$ [*De Pury and Farquhar*, 1997]. The leaf maximum carboxylation rate at 25°C $V_{c\max}$ is generally proportional to leaf nitrogen content and therefore is also a function of L:

$$V_{c\max}(L) = V_{c\max,0}\chi_n N(L) \tag{B2}$$

where $V_{c\max,0}$ is $V_{c\max}$ at the top of the canopy (i.e., $L = 0$), and χ_n defines the relative change of $V_{c\max}$ with N. N has a unit of g m^{-2}, and χ_n has a unit of m^2 g^{-1}. The values of χ_n, the mean values of $V_{c\max}$ and its standard deviation, and the mean values of N and its standard deviation for the various PFTs are provided in Table 1. The values at the top of the canopy, i.e., $V_{c\max,0}$ and N_0, are taken as their mean values plus one standard deviation.

[55] The fractions of sunlit and shaded leaf areas to the total leaf area vary with the depth into the canopy and can be described as:

$$f_{sun}(L) = e^{-kL} \tag{B3}$$

and

$$f_{sh}(L) = 1 - e^{-kL} \tag{B4}$$

where $k = G(\theta)\Omega/\cos\theta$, where $G(\theta)$ is the projection coefficient, usually taken as 0.5 for spherical leaf angle distribution, Ω is the clumping index, and θ is the solar zenith angle. Because these fractions vary with L, the mean values of leaf nitrogen content for sunlit and shaded leaves and their corresponding $V_{c\max}$ values can be obtained through vertical integrations with respect to L:

$$\begin{aligned} V_{c\max,sun} &= \frac{\int_0^L V_{c\max,0}\chi_n N(L) f_{sun}(L)dL}{\int_0^L f_{sun}(L)dL} \\ &= V_{c\max,0}\chi_n N_0 \frac{\int_0^L e^{-k_n L}e^{-kL}dL}{\int_0^L e^{-kL}dL} \\ &= V_{c\max,0}\chi_n N_0 \frac{k\left[1-e^{-(k_n+k)L}\right]}{(k_n+k)(1-e^{-kL})} \end{aligned} \tag{B5}$$

and

$$\begin{aligned} V_{c\max,sh} &= \frac{\int_0^L V_{c\max,0}\chi_n N(L) f_{sh}(L)dL}{\int_0^L f_{sh}(L)dL} \\ &= V_{c\max,0}\chi_n N_0 \frac{\int_0^L e^{-k_n L}\left(1-e^{-kL}\right)dL}{\int_0^L (1-e^{-kL})dL} \\ &= V_{c\max,0}\chi_n N_0 \frac{\frac{1}{k_n}\left[1-e^{-k_n L}\right] - \frac{1}{k_n+k}\left[1-e^{-(k_n+k)L}\right]}{L-\frac{1}{k}(1-e^{-kL})} \end{aligned} \tag{B6}$$

Equations (B5) and (B6) derived above are similar to those of *Wang and Leuning* [1998] but differ in detail because our leaf-to-canopy upscaling methodology is fundamentally different from their methodologies. They calculate canopy-level photosynthesis as the sum of two big-leaves, and therefore their vertical integrations result in the total accumulated values of photosynthetic capacity for the two big-leaves. Our methodology is to avoid using the big-leaf formulation by first obtaining the photosynthesis values of a representative sunlit leaf and a representative shaded leaf separately and multiplying them with their respective LAI (see equation (3)). Equations (B5) and (B6), therefore, represent the mean $V_{c\max}$ values for the representative sunlit and shaded leaves, respectively, obtained through weighting against sunlit and shaded leaf occurrence probabilities.

[56] After $V_{c\max}$ values for the representative sunlit and shaded leaves are obtained, the maximum electronic transport rate for the sunlit and shaded leaves are obtained from [*Wullschleger*, 1993]:

$$J_{\max,sun} = 29.1 + 1.64V_{c\max,sun} \tag{B7}$$

and

$$J_{\max,sh} = 29.1 + 1.64V_{c\max,sh} \tag{B8}$$

In this way, the effects of the vertical nitrogen gradient in the canopy on both the maximum carboxylation rate and the maximum electron transport rate are considered.

[57] **Acknowledgments.** This research is supported by a research grant (2010CB950704) under the Global Change Program of the Chinese Ministry of Science and Technology, an individual grant (GR-646) from the Canadian Foundation of Climate and Atmospheric Sciences (CFCAS) and the Canadian Carbon Program also funded by CFCAS. Several anonymous reviewers and the editor provided constructive comments that greatly improved this paper.

References

Alton, P. B., R. Ellis, S. O. Los, and P. R. North (2007), Improved global simulations of gross primary product based on a separate and explicit treatment of diffuse and direct sunlight, *J. Geophys. Res.*, *112*, D07203, doi:10.1029/2006JD008022.

Baker, D. F., et al. (2006), TransCom 3 inversion intercomparison: Impact of transport model errors on the interannual variability of regional CO_2 fluxes, 1988–2003, *Global Biogeochem. Cycles*, *20*, GB1002, doi:10.1029/2004GB002439.

Baldocchi, D. (1994), An analytical solution for coupled leaf photosynthesis and stomatal conductance models, *Tree Physiol.*, *14*, 1069–1079.

Baldocchi, D. D., and P. C. Harley (1995), Scaling carbon dioxide and water vapor exchange from leaf to canopy in a deciduous forest: Model testing and application, *Plant Cell Environ.*, *18*, 1157–1173, doi:10.1111/j.1365-3040.1995.tb00626.x.

Baldocchi, D. D., K. B. Wilson, and L. H. Gu (2002), How the environment, canopy structure and canopy physiological functioning influence carbon, water and energy fluxes of a temperate broad-leaved deciduous forest: An assessment with the biophysical model CANOAK, *Tree Physiol.*, *22*, 1065–1077, doi:10.1093/treephys/22.15-16.1065.

Ball, J. T. (1988), An analysis of stomatal conductance, PhD thesis, 89 pp., Stanford Univ., Stanford, Calif.

Baret, F., et al. (2006), Evaluation of the representativeness of networks of sites for the global validation and inter-comparison of land biophysical products: Proposition of the CEOS-BELMANIP, *IEEE Trans. Geosci. Remote Sens.*, *44*, 1794–1803, doi:10.1109/TGRS.2006.876030.

Baret, F., et al. (2007), LAI, fAPAR and fCover CYCLOPES global products derived from VEGETATION: Part 1: Principles of the algorithm, *Remote Sens. Environ.*, *110*, 275–286, doi:10.1016/j.rse.2007.02.018.

Beer, C., et al. (2010), Terrestrial gross carbon dioxide uptake: Global distribution and covariation with climate, *Science*, *329*, 834–838, doi:10.1126/science.1184984.

Black, T. A., J. M. Chen, X. Lee, and R. M. Sagar (1991), Characteristics of shortwave and longwave irradiances under a Douglas-fir forest stand, *Can. J. For. Res.*, *21*, 1020–1028, doi:10.1139/x91-140.

Bonan, G. B. (1991), A biophysical surface-energy budget analysis of soil-temperature in the boreal forests of Interior Alaska, *Water Resour. Res.*, *27*, 767–781, doi:10.1029/91WR00143.

Campbell, G. S., and J. M. Norman (1998), *An Introduction to Environmental Biophysics*, pp. 129–145, Springer, New York, doi:10.1007/978-1-4612-1626-1_9.

Canadell, J. G., C. Le Quéré, M. R. Raupach, C. B. Field, E. T. Buitehuis, P. Ciais, T. J. Conway, N. P. Gillett, R. A. Houghton, and G. Marland (2007), Contributions to accelerating atmospheric CO_2 growth from economic activity, carbon intensity, and efficiency of natural sinks, *Proc. Natl. Acad. Sci. U. S. A.*, *104*, 18,866–18,870, doi:10.1073/pnas.0702737104.

Chen, B., J. M. Chen, G. Mo, K. Yuan, K. Higuchi, and D. Chan (2007), Modeling and scaling coupled energy, water, and carbon fluxes based on remote sensing: An application to Canada's landmass, *J. Hydrometeorol.*, *8*, 123–143, doi:10.1175/JHM566.1.

Chen, B., J. M. Chen, G. Mo, and T. A. Black (2008), Comparison of regional carbon flux estimates from CO_2 concentration measurements and remote sensing based footprint integration, *Global Biogeochem. Cycles*, *22*, GB2012, doi:10.1029/2007GB003024.

Chen, J. M. (1996a), Canopy architecture and remote sensing of the fraction of photosynthetically active radiation in boreal conifer stands, *IEEE Trans. Geosci. Remote Sens.*, *34*, 1353–1368, doi:10.1109/36.544559.

Chen, J. M. (1996b), Optically based methods for measuring seasonal variation in leaf area index of boreal conifer forests, *Agric. For. Meteorol.*, *80*, 135–163, doi:10.1016/0168-1923(95)02291-0.

Chen, J. M., and T. A. Black (1992), Defining leaf area index for non-flat leaves, *Plant Cell Environ.*, *15*, 421–429, doi:10.1111/j.1365-3040.1992.tb00992.x.

Chen, J. M., and J. Cihlar (1995), Quantifying the effect of canopy architecture on optical measurements of leaf area index using two gap size analysis methods, *IEEE Trans. Geosci. Remote Sens.*, *33*, 777–787, doi:10.1109/36.387593.

Chen, J. M., and S. Leblanc (1997), A 4-scale bidirectional reflection model based on canopy architecture, *IEEE Trans. Geosci. Remote Sens.*, *35*, 1316–1337, doi:10.1109/36.628798.

Chen, J. M., and S. G. Leblanc (2001), Multiple-scattering scheme useful for hyperspectral geometrical optical modelling, *IEEE Trans. Geosci. Remote Sens.*, *39*, 1061–1071, doi:10.1109/36.921424.

Chen, J. M., T. A. Black, and R. S. Adams (1991), Evaluation of hemispherical photography for determining plant area index and geometry of a forest stand, *Agric. For. Meteorol.*, *56*, 129–143, doi:10.1016/0168-1923(91)90108-3.

Chen, J. M., P. M. Rich, T. S. Gower, J. M. Norman, and S. Plummer (1997), Leaf area index of boreal forests: Theory, techniques and measurements, *J. Geophys. Res.*, *102*, 29,429–29,443, doi:10.1029/97JD01107.

Chen, J. M., J. Liu, J. Cihlar, and M. L. Goulden (1999), Daily canopy photosynthesis model through temporal and spatial scaling for remote sensing applications, *Ecol. Modell.*, *124*, 99–119, doi:10.1016/S0304-3800(99)00156-8.

Chen, J. M., W. Ju, J. Cihlar, D. Price, J. Liu, W. Chen, J. Pan, T. A. Black, and A. Barr (2003), Spatial distribution of carbon sources and sinks in Canada's forests based on remote sensing, *Tellus, Ser. B*, *55*, 622–641, doi:10.1034/j.1600-0889.2003.00036.x.

Chen, J. M., C. H. Menges, and S. G. Leblanc (2005), Global derivation of the vegetation clumping index from multi-angular satellite data, *Remote Sens. Environ.*, *97*, 447–457, doi:10.1016/j.rse.2005.05.003.

Chen, J. M., F. Deng, and M. Chen (2006), Automated erratic cubic-spline capping method for reconstructing seasonal trajectories of a surface parameter derived from remote sensing, *IEEE Trans. Geosci. Remote Sens.*, *44*, 2230–2238, doi:10.1109/TGRS.2006.872089.

Chen, X., J. M. Chen, S. An, and W. Ju (2007), Effects of topography on simulated net primary productivity at landscape scale, *J. Environ. Manage.*, *85*, 585–596, doi:10.1016/j.jenvman.2006.04.026.

Cohen, S., R. S. Rao, and Y. Cohen (1997), Canopy transmittance inversion using a line quantum probe for a row crop, *Agric. For. Meteorol.*, *86*, 225–234, doi:10.1016/S0168-1923(96)02426-4.

Collatz, G. J., J. T. Ball, C. Crivet, and T. A. Berry (1991), Physiological and environmental regulation of stomatal conductance, photosynthesis and transpiration: A model that includes a laminar boundary layer, *Agric. For. Meteorol.*, *54*, 107–136, doi:10.1016/0168-1923(91)90002-8.

Cramer, W., et al. (1999), Comparing global models of terrestrial net primary productivity (NPP): Overview and key results, *Global Change Biol.*, *5*, 1–15, doi:10.1046/j.1365-2486.1999.00009.x.

Cramer, W., et al. (2001), Global response of terrestrial ecosystem structure and function to CO_2 and climate change: Results from six dynamic global vegetation models, *Global Change Biol.*, *7*, 357–373, doi:10.1046/j.1365-2486.2001.00383.x.

Demarez, V., S. Duthoit, F. Baret, M. Weiss, and G. Dedieu (2008), Estimation of leaf area and clumping indexes of crops with hemispherical photographs, *Agric. For. Meteorol.*, *148*, 644–655, doi:10.1016/j.agrformet.2007.11.015.

Demarty, J., F. Chevallier, A. D. Friend, N. Viovy, S. Piao, and P. Ciais (2007), Assimilation of global MODIS leaf area index retrievals within a terrestrial biosphere model, *Geophys. Res. Lett.*, *34*, L15402, doi:10.1029/2007GL030014.

Deng, F., J. M. Chen, S. Plummer, and M. Chen (2006), Global LAI algorithm integrating the bidirectional information, *IEEE Trans. Geosci. Remote Sens.*, *44*, 2219–2229.

De Pury, D. G. G., and G. D. Farquhar (1997), Simple scaling of photosynthesis from leaves to canopies without the errors of big-leaf models, *Plant Cell Environ.*, *20*, 537–557, doi:10.1111/j.1365-3040.1997.00094.x.

Erbs, D. G., S. A. Klein, and J. A. Duffie (1982), Estimation of diffuse radiation fraction for hourly, daily and monthly-averaged global radiation, *Sol. Energy*, *28*, 293–304.

Farquhar, G. D., S. von Caemmerer, and J. A. Berry (1980), A biochemical model of photosynthetic CO_2 assimilation in leaves of C3 species, *Planta*, *149*, 78–90, doi:10.1007/BF00386231.

Feng, X., G. Liu, J. M. Chen, M. Chen, J. Liu, W. Ju, R. Sun, and W. Zhou (2007), Simulating net primary productivity of terrestrial ecosystems in China using a process model driven by remote sensing, *J. Environ. Manage.*, *85*, 563–573, doi:10.1016/j.jenvman.2006.09.021.

Friedlingstein, P., et al. (2006), Climate-carbon cycle feedback analysis: Results from C4MIP model intercomparison, *J. Clim.*, *19*, 3337–3353, doi:10.1175/JCLI3800.1.

Garrigues, S., et al. (2008), Validation and intercomparison of global Leaf Area Index products derived from remote sensing data, *J. Geophys. Res.*, *113*, G02028, doi:10.1029/2007JG000635.

Goetz, S. J., S. D. Prince, J. Small, and A. C. R. Gleason (2000), Interannual variability of global terrestrial primary production: Results of a model driven with satellite observations, *J. Geophys. Res.*, *105*, 20,077–20,091, doi:10.1029/2000JD900274.

Goulden, M. L., B. C. Daube, S.-M. Fan, D. J. Sutton, A. Bazzaz, J. W. Munger, and S. C. Wofsy (1997), Physiological responses of a black spruce forest to weather, *J. Geophys. Res.*, *102*, 28,987–28,996, doi:10.1029/97JD01111.

Gurney, K. R., et al. (2002), Towards robust regional estimates of CO_2 sources and sinks using atmospheric transport models, *Nature*, *415*, 626–630, doi:10.1038/415626a.

Hanan, N. P., J. A. Berry, S. B. Verma, E. A. Walter-Shea, A. E. Suyker, G. G. Burba, and A. S. Denning (2005), Testing a model of CO_2, water and energy exchange in Great Plains tallgrass prairie and wheat ecosystems, *Agric. For. Meteorol.*, *131*, 162–179, doi:10.1016/j.agrformet.2005.05.009.

Hicke, J. A. (2005), NCEP and GISS solar radiation data sets available for ecosystem modeling: Description, differences, and impacts on net primary production, *Global Biogeochem. Cycles*, *19*, GB2006, doi:10.1029/2004GB002391.

Huete, A. R., K. Didan, Y. E. Shimabukuro, P. Ratana, S. R. Saleska, L. R. Hutyra, W. Yang, R. R. Nemani, and R. Myneni (2006), Amazon rainforests green-up with sunlight in dry season, *Geophys. Res. Lett.*, *33*, L06405, doi:10.1029/2005GL025583.

Hunt, E. R., Jr., and S. W. Running (1992), Simulated dry matter yields for aspen and spruce stand in the North American boreal forest, *Can. J. Remote Sens.*, *18*, 126–133.

Jarvis, P. G. (1976), The interpretation of the variations in leaf water potential and stomatal conductance found in canopies in the fields, *Philos. Trans. R. Soc. London, Ser. B*, *273*, 593–610, doi:10.1098/rstb.1976.0035.

Ju, W., J. M. Chen, T. A. Black, A. G. Barr, J. Liu, and B. Chen (2006), Modeling coupled water and carbon fluxes in a boreal aspen forest, *Agric. For. Meteorol.*, *140*, 136–151, doi:10.1016/j.agrformet.2006.08.008.

Kattge, J., W. Knorr, T. Raddatz, and C. Wirth (2009), Quantifying photosynthetic capacity and its relationship to leaf nitrogen content for global-scale terrestrial biosphere models, *Global Change Biol.*, *15*, 976–991, doi:10.1111/j.1365-2486.2008.01744.x.

Knorr, W., and M. Heimann (2001), Uncertainties in global terrestrial biosphere modeling: 1. A comprehensive sensitivity analysis with a new photosynthesis and energy balance scheme, *Global Biogeochem. Cycles*, *15*, 207–225, doi:10.1029/1998GB001059.

Krinner, G., N. Viovy, N. de Noblet-Ducoudré, J. Ogée, J. Polcher, P. Friedlingstein, P. Ciais, S. Sitch, and I. C. Prentice (2005), A dynamic global vegetation model for studies of the coupled atmosphere-biosphere system, *Global Biogeochem. Cycles*, *19*, GB1015, doi:10.1029/2003GB002199.

Lacaze, R., J. M. Chen, J.-L. Roujean, and S. G. Leblanc (2002), Retrieval of vegetation clumping index using hot spot signatures measured by multiangular POLDER instrument, *Remote Sens. Environ.*, *79*, 84–95, doi:10.1016/S0034-4257(01)00241-3.

Leblanc, S. G., J. M. Chen, H. P. White, R. Latifvic, J. R. Roujean, and R. Lacaze (2005a), Canada-wide foliage clumping index mapping from multi-angular POLDER measurements, *Can. J. Remote Sens.*, *31*, 364–376, doi:10.5589/m05-020.

Leblanc, S. G., J. M. Chen, R. Fernandes, D. W. Deering, and A. Conley (2005b), Methodology comparison for canopy structure parameters extraction from digital hemispherical photography in boreal forests, *Agric. For. Meteorol.*, *129*, 187–207, doi:10.1016/j.agrformet.2004.09.006.

Le Quéré, C., et al. (2009), Trends in the sources and sinks of carbon dioxide, *Nat. Geosci.*, *2*, 831–836, doi:10.1038/ngeo689.

Leuning, R. (1990), Modelling stomatal behaviour and photosynthesis of eucalyptus grandis, *Aust. J. Plant Physiol.*, *17*, 159–175, doi:10.1071/PP9900159.

Leuning, R. (1995), A critical appraisal of a combined stomatal-photosynthesis model for C3 plants, *Plant Cell Environ.*, *18*, 339–355, doi:10.1111/j.1365-3040.1995.tb00370.x.

Leuning, R., F. M. Kelliher, D. G. G. De Pury, and E.-D. Schulze (1995), Leaf nitrogen, photosynthesis, conductance and transpiration: Scaling from leaves to canopies, *Plant Cell Environ.*, *18*, 1183–1200, doi:10.1111/j.1365-3040.1995.tb00628.x.

Li, K. Y., R. De Jong, and J. B. Boisvert (2001), An exponential root-water-uptake model with water stress compensation, *J. Hydrol.*, *252*, 189–204, doi:10.1016/S0022-1694(01)00456-5.

Liu, J., J. M. Chen, J. Cihlar, and W. M. Park (1997), A process-based boreal ecosystem productivity simulator using remote sensing inputs, *Remote Sens. Environ.*, *62*, 158–175, doi:10.1016/S0034-4257(97)00089-8.

Matsushita, B., and M. Tamura (2002), Integrating remotely sensed data with an ecosystem model to estimate net primary productivity in East Asia, *Remote Sens. Environ.*, *81*, 58–66, doi:10.1016/S0034-4257(01)00331-5.

Matsushita, B., M. Xu, J. Chen, S. Kameyama, and M. Tamura (2004), Estimation of regional net primary productivity (NPP) using a process-based ecosystem model: How important is the accuracy of climate data?, *Ecol. Modell.*, *178*, 371–388, doi:10.1016/j.ecolmodel.2004.03.012.

Medlyn, B. E., et al. (1999a), Effects of elevated [CO2] on photosynthesis in European forest species: A meta-analysis of model parameters, *Plant Cell Environ.*, *22*, 1475–1495, doi:10.1046/j.1365-3040.1999.00523.x.

Medlyn, B., et al. (1999b), Meta-analysis of model parameters, in *Predicted Impacts of Rising Carbon Dioxide and Temperature on Forests in Europe at Stand Scale*, *Final Rep. ENV4-CT95-0077 IC20-CT96-0028*, ECOCRAFT Environ. Res. and Dev., Univ. of Edinburgh, Edinburgh, U. K.

Miller, E. E., and J. M. Norman (1971a), Sunfleck theory for plant canopies 1. Lengths of sunlit segments along a transect, *Agron. J.*, *63*(5), 735–738.

Miller, E. E., and J. M. Norman (1971b), Sunfleck theory for plant canopies 2. Penumbra effect: Intensity distributions along sunfleck segments, *Agron. J.*, *63*(5), 739–743, doi:10.2134/agronj1971.00021962006300050025x.

Morisette, J. T., et al. (2006), Validation of global Moderate-Resolution LAI products: A framework proposed within the CEOS land product validation subgroup, *IEEE Trans. Geosci. Remote Sens.*, *44*, 1804–1817, doi:10.1109/TGRS.2006.872529.

Myneni, R. B., et al. (2002), Global products of vegetation leaf area and fraction absorbed PAR from one year of MODIS data, *Remote Sens. Environ.*, *83*, 214–231, doi:10.1016/S0034-4257(02)00074-3.

Nilson, T. (1971), A theoretical analysis of the frequency of gaps in plant stands, *Agric. Meteorol.*, *8*, 25–38, doi:10.1016/0002-1571(71)90092-6.

Niu, S., Z. Yuan, Y. Zhang, W. Liu, L. Zhang, J. Huang, and S. Wan (2005), Photosynthetic responses of C3 and C4 species to seasonal water variability and competition, *J. Exp. Bot.*, *56*, 2867–2876, doi:10.1093/jxb/eri281.

Norman, J. M. (1982), Simulation of microclimates, in *Biometeorology in Integrated Pest Management*, edited by J. L. Hatfield and I. J. Thomason, pp. 65–99, Academic, San Diego, Calif.

Norman, J. M., and P. G. Jarvis (1974), Photosynthesis in sitka spruce (Picea-sitchensis (Bong) carr) 3. Measurements of canopy structure and interception of radiation, *J. Appl. Ecol.*, *11*, 375–398, doi:10.2307/2402028.

Norman, J. M., and J. M. Welles (1983), Radiative transfer in an array of canopies, *Agron. J.*, *75*, 481–488, doi:10.2134/agronj1983.00021962007500030016x.

Piao, S., P. Ciais, P. Friedlingstein, N. de Noblet-Ducoudré, P. Cadule, N. Viovy, and T. Wang (2009), Spatiotemporal patterns of terrestrial carbon cycle during the 20th century, *Global Biogeochem. Cycles*, *23*, GB4026, doi:10.1029/2008GB003339.

Pisek, J., and J. M. Chen (2007), Comparison and validation of MODIS and VEGETATION global LAI products over four BigFoot sites in North America, *Remote Sens. Environ.*, *109*, 81–94, doi:10.1016/j.rse.2006.12.004.

Pisek, J., J. M. Chen, and F. Deng (2007), Canada-wide validation of a new global leaf area index dataset from SPOT-4 VEGETATION data, *Can. J. Remote Sens.*, *33*, 1–16.

Pisek, J., J. M. Chen, R. Lacaze, O. Sonnentag, and K. Alikas (2010), Expanding global mapping of foliage clumping index with multi-angular POLDER 3 measurements: Evaluation and topographic compensation, *ISPRS J. Photogramm. Remote Sens.*, *65*, 341–346, doi:10.1016/j.isprsjprs.2010.03.002.

Potter, C. S., J. T. Randerson, C. B. Field, P. A. Matson, P. M. Vitousek, H. A. Mooney, and S. A. Klooster (1993), Terrestrial ecosystem production: A process model based on global satellite and surface data, *Global Biogeochem. Cycles*, *7*, 811–841, doi:10.1029/93GB02725.

Prihodko, L., A. S. Denning, and I. Baker (2005), Modelling drought tolerance in Amazonia with SiB3, paper presented at Seventh International Carbon Dioxide Conference, Boulder, Colo., 25–30 Sept.

Radcliffe, D., T. Hayden, K. Watson, P. Crowley, and R. E. Phillips (1980), Simulation of soil-water within the root zone of a corn crop, *Agron. J.*, *72*, 19–24, doi:10.2134/agronj1980.00021962007200010005x.

Rayner, P. J., R. M. Law, C. E. Allison, R. J. Francey, C. M. Trudinger, and C. Pickett-Heaps (2008), Interannual variability of the global carbon cycle (1992–2005) inferred by inversion of atmospheric CO_2 and $\delta^{13}CO_2$ measurements, *Global Biogeochem. Cycles*, *22*, GB3008, doi:10.1029/2007GB003068.

Roujean, J.-L., and R. Lacaze (2002), Global mapping of vegetation parameters from POLDER multiangular measurements for studies of surface-atmosphere interactions: A pragmatic method and its validation, *J. Geophys. Res.*, *170*(D12), 4150, doi:10.1029/2001JD000751.

Ruimy, A., G. Dedieu, and B. Saugier (1996), TURC: A diagnostic model of continental gross primary productivity and net primary productivity, *Global Biogeochem. Cycles*, *10*, 269–285, doi:10.1029/96GB00349.

Running, S. W., R. R. Nemani, F. A. Heinsch, M. Zhao, M. Reeves, and H. Hashimoto (2004), A continuous satellite-derived measure of global terrestrial primary production, *BioScience*, *54*, 547–560, doi:10.1641/0006-3568(2004)054[0547:ACSMOG]2.0.CO;2.

Ryu, Y., T. Nilson, H. Kobayashi, O. Sonnentag, B. E. Law, and D. D. Baldocchi (2010a), On the correct estimation of effective leaf area index: Does it reveal information on clumping effects?, *Agric. For. Meteorol.*, *150*(3), 463–472, doi:10.1016/j.agrformet.2010.01.009.

Ryu, Y., O. Sonnentag, T. Nilson, R. Vargas, H. Kobayashi, R. Wenk, and D. D. Baldocchi (2010b), How to quantify tree leaf area index in an open savanna ecosystem: A multi-instrument and multi-model approach, *Agric. For. Meteorol.*, *150*, 63–76, doi:10.1016/j.agrformet.2009.08.007.

Saigusa, N., et al. (2008), Temporal and spatial variations in the seasonal patterns of CO_2 flux in boreal, temperate, and tropical forests in East Asia, *Agric. For. Meteorol.*, *148*, 700–713, doi:10.1016/j.agrformet.2007.12.006.

Saxton, K. E., W. J. Rawls, J. S. Romberger, and R. I. Papendick (1986), Estimating generalized soil-water characteristics from texture, *Soil Sci. Soc. Am. J.*, *50*, 1031–1036, doi:10.2136/sssaj1986.03615995005000040039x.

Schieving, F. (1998), *Plato's Plant: On the Mathematical Structure of Simple Plants and Canopies*, 360 pp. Backhuys, Leiden, Netherlands.

Schulze, E.-D., and D. S. S. Schimel (2001), Uncertainties of global biogeochemical predictions, in *Global Biogeochemical Cycles in the Climate System*, edited by E.-D. Schulze et al., pp. 1–14, Academic, San Diego, Calf.

Schwalm, C. R., et al. (2010), A model-data intercomparison of CO_2 exchange across North America: Results from the North America Carbon Program site synthesis, *J. Geophys. Res.*, *115*, G00H05, doi:10.1029/2009JG001229.

Sonnentag, O., J. Talbot, J. M. Chen, and T. N. Roulet (2007), Using direct and indirect measurements of leaf area index to characterize the shrub canopy of an ombrotrophic peatland, *Agric. For. Meteorol.*, *144*, 200–212, doi:10.1016/j.agrformet.2007.03.001.

Spitters, C. J. T., H. A. J. M. Toussaint, and J. Goudriaan (1986), Separating the diffuse and direct component of global radiation and its implications for modeling canopy photosynthesis. Part I. Components of incoming radiation, *Agric. For. Meteorol.*, *38*(1–3), 217–229, doi:10.1016/0168-1923(86)90060-2.

Sprintsin, M., J. M. Chen, A. R. Desai, and C. M. Gough (2012), Evaluation of leaf-to-canopy upscaling methodologies against carbon flux data in North America, *J. Geophys. Res.*, doi:10.1029/2010JG001407, in press.

Sterck, F. J., and F. Schieving (2007), 3-D growth patterns of trees: Effects of carbon economy, meristem activity, and selection, *Ecol. Monogr.*, *77*, 405–420, doi:10.1890/06-1670.1.

Still, C. J., J. A. Berry, G. J. Collatz, and R. S. DeFries (2003), Global distribution of C_3 and C_4 vegetation: Carbon cycle implications, *Global Biogeochem. Cycles*, *17*(1), 1006, doi:10.1029/2001GB001807.

Wang, Q., J. Tenhunen, E. Falge, C. Bernhofer, A. Granier, and T. Vesalas (2003), Simulation and scaling of temporal variation in gross primary production for coniferous and deciduous temperate forests, *Global Change Biol.*, *10*, 37–51, doi:10.1046/j.1529-8817.2003.00716.

Wang, S., J. M. Chen, W. Ju, X. Feng, M. Chen, P. Chen, and G. Yu (2007), Carbon sinks and sources in China's forests during 1901–2001, *J. Environ. Manage.*, *85*, 524–537, doi:10.1016/j.jenvman.2006.09.019.

Wang, Y.-P., and R. Leuning (1998), A two-leaf model for canopy conductance, photosynthesis and partitioning of available energy I: Model description and comparison with a multi-layered model, *Agric. For. Meteorol.*, *91*, 89–111, doi:10.1016/S0168-1923(98)00061-6.

Webb, R. S., C. E. Rosenzweig, and E. R. Levine (1991), A global data set of soil particle size properties, *NASA Tech. Memo.*, *TM-4286*, 40 pp.

Williams, M., et al. (1996), Modeling the soil-plant-atmosphere continuum in a Quercus-Acer stand at Harvard forest: The regulation of stomatal conductance by light, nitrogen and soil/plant hydraulic properties, *Plant Cell Environ.*, *19*, 911–927, doi:10.1111/j.1365-3040.1996.tb00456.x.

Wullschleger, S. D. (1993), Biochemical limitations to carbon assimilation in C_3 plants: A retrospective analysis of the A/C_i curves from 109 species, *J. Exp. Bot.*, *44*, 907–920, doi:10.1093/jxb/44.5.907.

Zhao, M., and S. W. Running (2010), Drought-induced reduction in global terrestrial net primary production from 2000 through 2009, *Science*, *329*, 940–943, doi:10.1126/science.1192666.

Zhao, M., S. W. Running, and R. R. Nemani (2006), Sensitivity of Moderate Resolution Imaging Spectroradiometer (MODIS) terrestrial primary production to the accuracy of meteorological reanalyses, *J. Geophys. Res.*, *111*, G01002, doi:10.1029/2004JG000004.

Zheng, G., J. M. Chen, Q. Tian, W. M. Ju, and X. Xia (2007), Combining remote sensing imagery and forest age inventory for biomass mapping, *J. Environ. Manage.*, *85*, 616–623, doi:10.1016/j.jenvman.2006.07.015.

Zhou, Y., Q. Zhu, J. M. Chen, Y. Q. Wang, J. Liu, R. Sun, and S. Tang (2007), Observation and simulation of net primary productivity in Qilian mountain, Western China, *J. Environ. Manage.*, *85*, 574–584, doi:10.1016/j.jenvman.2006.04.024.

Zierl, B. (2001), A water balance model to simulate drought in forested ecosystems and its application to the entire forested area in Switzerland, *J. Hydrol.*, *242*, 115–136, doi:10.1016/S0022-1694(00)00387-5.

D. Chan and M. Ishizawa, Meteorological Service of Canada, Environment Canada, 4905 Dufferin St., Toronto, ON M3H 5T4, Canada.

J. M. Chen, J. Liu, G. Mo, and J. Pisek, Department of Geography, University of Toronto, 100 St. George St., Toronto, ON M5S 3G3, Canada. (chenj@geog.utoronto.ca)

F. Deng, International Institute of Earth System Science, Nanjing University, 22 Hankou Road, Nanjing, Jiangsu 210093, China.